

Local Bulk Composition Effects on Metamorphic Mineral Assemblages

Pierre Lanari and Martin Engi

*Institute of Geological Sciences
University of Bern
Baltzerstrasse 3
CH-3012 Bern
Switzerland*

*pierre.lanari@geo.unibe.ch
martin.engi@geo.unibe.ch*

INTRODUCTION AND SCOPE

Plate tectonic forcing leads to changes in the physical conditions that affect the lithosphere. In response to such changes, notably the local temperature (T) and pressure (P), rocks evolve dynamically. Processes mostly involve mineral transformations, i.e., solid-state reactions, but (hydrous) fluids are often involved, and partial melting may occur in the Earth's middle and lower crust. While these chemical reactions reflect the tendency of natural systems to reduce their Gibbs free energy, metamorphic rocks commonly preserve textural and mineralogical relics, such as compositionally zoned minerals. Where relics are present, thermodynamic equilibrium clearly was not attained during the evolution of the rock.

Petrochronology seeks to establish a temporal framework of petrologic evolution, and for this purpose it is essential to determine the P – T conditions prevailing at several stages. When analyzing a rock sample it is thus critical:

- (a) to recognize whether several stages of its evolution can be discerned,
- (b) to document the minerals that formed or were coexisting at each stage, and
- (c) to estimate at what physical conditions this happened.

If (and only if) a chronometer then can be associated to one of these stages—or better yet several chronometers to different stages—then the power of petrochronology becomes realizable.

This chapter is concerned with a basic dilemma that results directly from steps (b) and (c) above: P – T conditions are determined on the basis of mineral barometers and thermometers, which mostly rest on the assumption of chemical (or isotopic) equilibrium, yet the presence of relics is proof that thermodynamic equilibrium was not attained. One way out of the dilemma is to analyze reaction mechanisms and formulate a model based on non-equilibrium thermodynamics and kinetics (Lasaga 1998). While this can be fruitful for understanding fundamental aspects of metamorphic petrogenesis, there are more direct ways to address the limited scope needed for petrochronology. The alternative pursued here seeks to define the scale(s) of equilibration, i.e., to determine spatial limits within which chemical equilibration can reasonably be assumed.

The past fifty years have seen rapid developments in forward thermodynamic models aimed at retrieving the conditions of equilibration from local assemblages. These models are rooted in chemical equilibrium theory—the concept that rocks successively re-equilibrate along

at least part of their evolution or remain at least close to chemical equilibrium. Since the advent of electron probe micro-analysis (EPMA), mineral chemical data have been combined with textural observations in thin section, and in many rocks different local mineral assemblages have been documented. The question is what caused these differences: Do they represent temporally distinct stages of a single chemical system or coeval domains of locally different chemical composition? This question is known as the *N*-dimensional tie-line problem (Greenwood 1967): Can two mineral assemblages be related to one another by a balanced chemical reaction or must the observed differences in their mineralogy be attributed to differing bulk compositions? A rigorous answer is possible,¹ provided the frozen-in assemblages reflect chemical equilibrium at the time of formation—a hypothesis to be tested. In any case, equilibrium assemblages reflect the chemical composition of rocks, and for forward chemical modeling of assemblages that composition must be known. Textural evidence in polymineralic rocks typically suggests some chemical heterogeneity, as the modal distributions of the minerals (i.e., their volumetric abundance) commonly varies at centimeter- to millimeter-scale, or less. Chemical heterogeneity can be inherited, e.g., from interlayered strata, or it may form during metamorphism, by metamorphic differentiation (Orville 1969). Either way, the effects of chemical heterogeneity should be considered in forward modeling, especially in clearly domainal rocks. As petrochronological studies focus on dating minerals in their local context, petrogenetic conditions ought to be reliably determined by modeling at similarly small scale.

This paper examines some of the major causes for and consequences of chemical heterogeneity in rocks, which can affect the scale of equilibration and thus the modeled mineral assemblages. The central question addressed is: how can a realistic bulk composition be found, such that model results can be compared in detail to a documented sample? A completely systematic treatment is beyond the scope of this paper, but as some fundamental aspects are involved in applying equilibrium thermodynamics to metamorphic rocks, the necessary basics are presented in the first section. Some of the case studies discussed in the second half of this paper also invoke kinetic aspects. These are cited where necessary but are not reviewed here; several resources treat the kinetics of metamorphic processes (see for example the book of Lasaga 1998). In the following sections we analyze specific cases such as the porphyroblastic growth of garnet that fractionates the reactive bulk composition and the link with mineral inclusion chronology. We also develop in a more general way the formation and evolution of textural domains in rocks, including the chemical subsystems and potential gradients. In the last section, we review analytical methods to estimate local bulk compositions using standardized X-ray maps (and the program XMapTools, Lanari et al. 2014b). We then show some applications to petrochronological analysis, and we outline perspectives for future research.

THEORETICAL BASIS AND LIMITS OF FORWARD THERMODYNAMIC ANALYSIS

Based on the pioneering work of Bowen (1913) and Goldschmidt (1911), equilibrium thermodynamics has proven a powerful conceptual framework to develop forward chemical modeling. Recent progress in the accuracy and efficiency of such techniques has had a major impact on the evolution of metamorphic petrology (Spear et al. 2016). It now is straightforward to model at least some of the main transformational stages experienced by crystalline rocks (Yakymchuk et al. 2017, this volume and references therein). Many of the previously daunting technical obstacles, such as the need for sophisticated solution models in complex systems involving solid and fluid phases, now appear much less evident, as the available software is making use of thermodynamic databases. However, despite periodic updates of such databases,

¹ Greenwood showed that linear algebraic examination is sufficient to determine whether two samples (or assemblages) overlap in composition space. If they do, yet they show different assemblages, this necessarily reflects a difference in physical conditions (e.g., of pressure or temperature).

models for some mineral systems remain imperfectly calibrated. For many bulk compositions predicted phase relations are reliably known, but for others the models may be partly flawed, and this is easily overlooked. Furthermore, predictions based on classical thermodynamics are limited to systems in equilibrium, and the application to metamorphic rocks is not self-evident where they contain non-equilibrium phenomena. In particular, the definition of an appropriate equilibration volume suitable for modeling can be a challenging task, as natural rocks typically record several stages of the metamorphic history through compositional zoning, mineral relics and textural relationships. Nevertheless, our current understanding of the metamorphic processes in the Earth's crust has much improved due to the comparison of model predictions with the observed mineral assemblages and compositions. Such predictions rely on the application of forward chemical modeling based on the bulk rock composition of natural samples. In a recent review, Powell and Holland (2010) concluded that "the success of using forward equilibrium model to study metamorphic rocks provides, at least in part, an *a posteriori* justification of the assumption" [of equilibrium]. On the other hand, some authors have warned the community about the limits of equilibrium models and have demonstrated, for instance, that kinetic impediments to reaction may prevent metamorphic rocks from attaining rock-wide chemical equilibrium along their prograde crystallization paths (Carlson et al. 2015 and references therein). It is also increasingly recognized that nucleation and growth can be kinetically inhibited (Gaidies et al. 2011; Spear et al. 2014), and so models based on reaction affinity rather than equilibrium thermodynamics may be required.

Gibbs free energy minimization

The equilibrium phase assemblage in a chemically closed system for any specified set of conditions is classically determined using the principle of Gibbs free energy minimization. The chemical equilibrium condition of any system of fixed composition is:

$$\text{minimize } G_{\text{system}} = \sum_k n_k g_k \quad (1)$$

where n_k is the number of moles and g_k the molar Gibbs free energy of phase k . The interested reader would note that this chemical equilibrium condition is subject to two additional constraints: (1) all $n_k \geq 0$ with $\sum n_k = 1$ and (2) the mass balance equations (e.g., $\sum x_k^i n_k = x_{\text{system}}^i$ for component i with x_k^i the composition in phase k) are satisfied. The computation of the equilibrium phase assemblage requires values for the molar Gibbs free energy of pure phases and a formulation of the relation between composition and activity for each solution phase. Consequently Gibbs free energy minimization relies on thermodynamic data for the standard state thermodynamic properties, PVT -equations of state, and solution models for solids and fluids. Successful application of forward equilibrium models requires an internally consistent thermodynamic database with accurate solution models and a robust estimate for the bulk composition of the system.

The development and successive improvements of internally-consistent thermodynamic databases for solid and fluids (Berman 1988; Holland and Powell 1988, 1998, 2011; Gottschalk 1996; Miron et al. 2016) are one of the greatest advances in the field of metamorphic petrology in the last three decades. Using the Gibbs free energy minimization principle, these databases facilitate the creation of phase diagrams that describe which mineral phases are stable as a function of temperature (T), pressure (P), H_2O and CO_2 activity (a_{H_2O} , a_{CO_2}), oxygen fugacity (f_{O_2}) or chemical potential of a component i (μ_i). A significant move occurred in the late 80's with the development of modeling programs including Thermocalc (Powell et al. 1998; Powell and Holland 2008), Perple_X (Connolly 1990, 2005) and Theriak-Domino (De Capitani and Brown 1987; de Capitani and Petrakakis 2010). Such programs can be used to generate isochemical equilibrium phase diagrams (elsewhere called 'pseudosection', but this term may engender confusion as noted by Spear et al. 2016), which map assemblages predicted at minimum free energy for the chemical system of interest (Eqn. 1). It is owing to the remarkable power and availability of these programs that isochemical equilibrium phase diagrams have become so widely used.

The concept of chemical equilibrium and its application to metamorphic rocks

A volume of rock is said to be in chemical equilibrium when the quantities and compositions of the phases involved do not change in time without an external influence. Equilibrium is a macroscopic concept that is defined in terms of macroscopic variables such as P , T and chemical potential (or activity or composition) in the considered system, which is commonly known as the equilibration volume. It is important to note that the macroscopic variables are large-scale average quantities, which are subject to fluctuations at a microscopic scale. Equilibrium thermodynamics requires that, in response to any change in P – T conditions, the equilibration volume (with a given composition vector \mathbf{x}) will adjust its phase assemblage, i.e., the modes and compositions of all minerals, in an attempt to reach or maintain chemical equilibrium. By definition, the principles of chemical equilibrium predict the final state of a system, independent of the path by which the system arrived at its present state (see below).

A schematic thin section of metapelite consisting of Grt+Chl+Ms+Bt+Pl+Qz+H₂O (mineral abbreviations are from Whitney and Evans 2010) at ~525 °C and 6 kbar is shown in Figure 1a. The mineral phases are assumed to be homogeneous in composition and coexist at chemical equilibrium for the given P – T conditions. Any increase in P or T would require

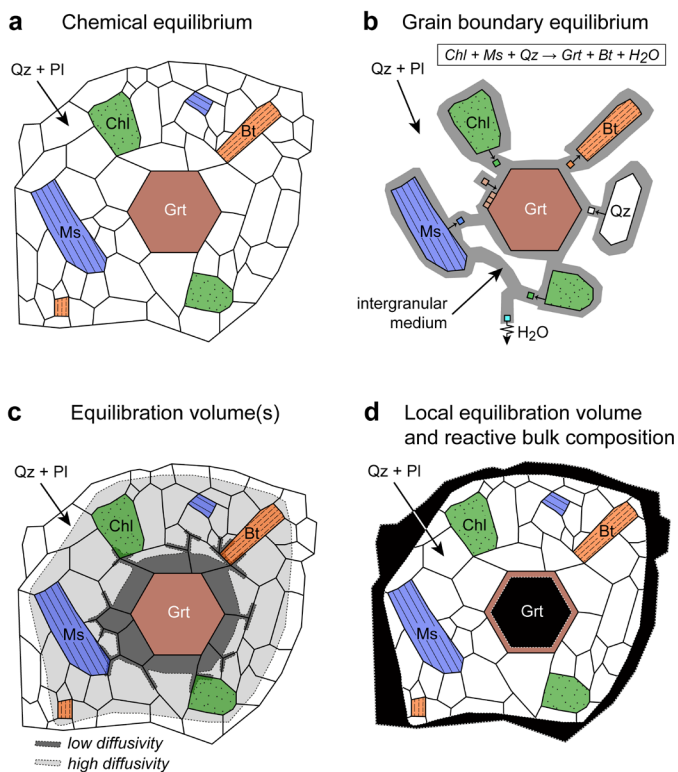


Figure 1. Schematic thin section consisting of garnet, chlorite, muscovite, biotite in a quartz–plagioclase matrix. (a) Chemical equilibrium model: all mineral phases are homogeneous and coexist in equilibrium at the P – T conditions of interest. (b) Grain boundary equilibrium model and assemblage re-equilibration under higher temperature conditions through the reaction $\text{Chl} + \text{Ms} + \text{Qz} \rightarrow \text{Grt} + \text{Bt} + \text{H}_2\text{O}$. (c) Two equilibrium volumes are shown, one for an element (dark gray) with low diffusivity, a second one (light gray) assuming fast transport. (d) The local equilibrium volume involves only the rim of the zoned minerals (here garnet) and a homogeneous domain (matrix) of a section. The reactive bulk composition is the composition of the local equilibrium volume, which excludes the domains shown in black.

adjustments through the reaction $\text{Chl} + \text{Ms} + \text{Qz} \rightarrow \text{Grt} + \text{Bt} + \text{H}_2\text{O}$ (Fig. 1b) to attain a new equilibrium state. As the solid-state transformations are achieved by dissolution, precipitation and transport of the elemental species through the intergranular medium, the problem can be reduced to a grain boundary equilibrium model. This concept is a step forward in the application of chemical equilibrium theory to analyze metamorphic rocks but it requires an approximation of the bulk composition of the intergranular medium. However some fundamental concerns appear as soon as we abandon this idealized scenario. Most of them are related to the size and the composition of the equilibration volume. From a theoretical point of view, transport and reaction kinetics can establish and maintain chemical potential gradients in the system and avoid the achievement of chemical equilibrium, i.e., an equilibration volume cannot be defined. An additional concern comes from the observation that a metamorphic rock is seldom truly homogeneous and often contains evidence of disequilibrium, even at grain-scale, such as chemical zoning or mineral relics. In this case it can be challenging to define an appropriate equilibration volume to be modeled. Those cases are separately addressed below.

Reaction kinetics. Equilibrium thermodynamic models in closed systems are based on the equilibrium condition (Eqn. 1), and they neglect the fact that solid-state reactions cannot strictly proceed to equilibrium (Carlson et al. 2015 and references therein) simply because the driving force—chemical potential gradients between reactants and products—would be eliminated. Consequently, equilibrium thermodynamics ignores (1) the time-courses of mineral assemblage transformations, (2) the specific mechanism by which rocks crystallize, and (3) the rate at which that crystallization occurs. Any evolution of texture from metastable states to a stable state is a transient feature, and intermediate states are completely obliterated if the rock reaches equilibrium. From a microscopic point of view, the successive transformations are achieved via re-equilibration, e.g., dissolution and precipitation or pseudomorphic replacement of mineral phases and by inter- and intragranular diffusion of the chemical components (Fig. 1b). The driving forces for diffusion are the chemical potential gradients that are established between minerals such as the reactants and products of a metamorphic reaction or between different groups of minerals, such as between domains (Fisher 1973). In this context, equilibration is attained when the chemical potentials of each the chemical component in the system of interest is equalized across a rock. Several studies on equilibrium have demonstrated that deformation and fluid influx can help to achieve equilibration (Brodie and Rutter 1985; Wintsch 1985; Foster 1991; Erambert and Austrheim 1993).

Frozen chemical potential gradients. The modeling of rock volumes that attained chemical equilibrium, such as shown in the idealized scenario of Figure 1a, is relatively straightforward using Equation (1) and an appropriate thermodynamic database. However, nature provides abundant examples of diffusion-controlled structures such as coronas, which typically result from incomplete metamorphic transformation due to low rates of elemental movement by intragranular diffusion. Indeed chemical zoning in coronas may also reflect chemical potential gradients, which must be distinguished from zoning due to changes in P - T conditions (Indares and Rivers 1995). Diffusion-controlled structures can be identified in thin section because they typically have a strong spatial organization with textural mineral zones showing sharp changes in compositions at zone boundaries. Reaction fronts are arranged in an orderly sequence of increasing or decreasing chemical potential (Fisher 1973). Non-equilibrium thermodynamics (also known as non-classical or irreversible thermodynamics) has been used to analyze such inhomogeneous systems; their study requires the knowledge of the rates of reactions (Fisher 1973; Foster 1977, 1986, 1999; Fisher and Lasaga 1981; Johnson and Carlson 1990; Carlson and Johnson 1991; Lasaga 1998).

Mineral compositional zoning and mineral relics. Growth related compositional zoning and mineral relics are clear evidence of disequilibrium in metamorphic rocks. It was recognized early after the introduction of the EPMA to the geosciences that garnet porphyroblasts can

freeze compositional zoning (Hollister 1966). Such textures reflect changes in P – T conditions, indicating that the crystal as a whole did not equilibrate with the matrix during growth (Atherton 1968; Tracy et al. 1976). In such cases some part of the minerals that formed earlier (e.g., garnet) is effectively removed from the reactive part of the rock (the effects of metamorphic fractionation are intensely discussed below, in the section related to garnet porphyroblast growth). A few years later, Tracy (1982) reported a list of 18 metamorphic minerals showing similar compositional zoning. As most metamorphic rocks exhibit compositionally zoned minerals, equilibrium at best was established at a local scale only (Fig. 1c). Hence, to apply equilibrium thermodynamics, more sophisticated models are required.

The principle of local equilibrium. The principle of local equilibrium (or mosaic equilibrium) restricts the investigation to subsystems that are small enough that the attainment of an equilibrium state can be assumed (Korzhinskii 1936, 1959; Thompson 1955, 1959, 1970). Local equilibrium is considered only at a scale over which variations in chemical potential—and all physical variables—are negligible. Since chemical heterogeneity in a sample is primarily evident in solid solutions, local equilibria address only those situations where the minerals (or individual zones thereof) are chemically uniform. The principle of local equilibrium significantly extends thermodynamic modeling to cases that would otherwise require a kinetic description (White et al. 2008). This includes, as we shall see, the domain in which chemical potential gradients were frozen in and the mineral relics (e.g., cores) were isolated from the reactive part of the rock. The concept of local equilibrium is thus useful for forward equilibrium models, but it demands that we define the equilibration volume to be investigated.

Bulk rock composition vs reactive bulk composition

In the literature of metamorphic petrology, the term bulk rock composition generally refers to the average chemical composition of a whole-rock sample analyzed, for example by X-ray fluorescence spectrometry (XRF). In the framework of local equilibrium, the analysis can be restricted to a specific region or domain—its size often is less than thin-section scale—in a rock, chosen for its uniform chemical composition (or mineral modes). In this case we refer to the concept of local bulk composition. Note that bulk rock compositions and local bulk compositions are measured quantities and may or may not be relevant for modeling, i.e., representative of the equilibrium volume to be investigated.

Various studies over the past 15 years struggled to define a relevant bulk composition for a given sample situation, and this question typically was raised when models using the bulk rock composition rendered unrealistic results (e.g., Warren and Waters 2006). As discussed above, the relevant bulk composition of a rock for equilibrium models is the composition of the (presumed) equilibration volume at a specific stage of the evolution, and it may exclude certain refractory or inert minerals that are observed in a domain, but may be shielded from reactions. The composition of the equilibration volume is known as the effective bulk composition or reactive bulk composition (Fig. 1d). The term effective bulk composition was originally introduced by Tracy (1982) and reused in several studies (Hickmott et al. 1987; Spear 1988b; Stüwe 1997; Marmo et al. 2002; Evans 2004; Tinkham and Ghent 2005a), but in the following we decided to use the term reactive bulk composition as it is most descriptive in a modeling framework. As will be demonstrated below in the section on garnet porphyroblast growth, the reactive bulk composition changes along a P – T trajectory because of compositional fractionation (Tracy 1982; Spear 1988b; Spear et al. 1990).

Open questions on bulk composition effects and the size of equilibration volume

Forward equilibrium models based on the assumption of local equilibrium require the use of reactive bulk compositions, which in some favorable cases can be approximated by local bulk compositions or calculated using fractional crystallization models. The choice of an appropriate or representative rock or domain composition can be critical, as it may significantly

affect the results of modeling. Aware of the perils, Kelsey and Hand (2015) warned that “this topic is in some ways like the elephant in the room”. The question is: How sensitive are predictions made by equilibrium models to variations in the bulk rock composition? Detailed investigations have been conducted at the regional scale (Tinkham et al. 2001; White et al. 2003), but it appears that only a few studies have explicitly addressed this question at the sample scale. The paucity of knowledge is due in part to the difficulty of estimating uncertainties in the bulk rock composition and then propagating their effect.

Are realistic equilibration volumes impossible to identify exactly, as claimed by Stüwe (1997)? Despite many studies over more than 25 years (e.g., Powell and Downes 1990; Vance and Mahar 1998; Brown 2002; Marmo et al. 2002; Powell et al. 2005), it remains intriguing which parameters control the size of the equilibration volume. Some progress has been made in accounting for phases that should be included or excluded from the equilibration volume (Lanari et al. 2017). If an intergranular medium (specifically a fluid) is present in a rock, transport distances of dissolved species in this medium are critical (Carlson 2002); but what if mobility was limited to volume diffusion? Orders of magnitude difference in transport result from this uncertainty, especially in highly deformed rocks, since strain can increase the dislocation density, reactivity, and transport rates. In any case, diffusion rates are temperature-dependent, so equilibration volume is expected to increase during heating (and drastically decrease upon cooling, as rocks tend to “dry up”), and as shown in Figure 1c, it may differ substantially for different chemical species (Carlson 1989; Spear and Daniel 2001). This is particularly critical for some of the trace elements relevant to petrochronology (e.g., Gatewood et al. 2015). An essential parameter controlling the extent of local (dis)equilibrium is the rate at which local reactions proceed towards equilibrium compared to the rate of change in physical parameters (P - T - X , e.g., the heating rate). If kinetics are favorable, the system can respond rapidly by adjusting the mode (i.e., the volumetric abundance) and composition of each phase in the assemblage to the P - T - X conditions of the equilibration volume; if so, all the minerals in that domain will be stable at the same reactive bulk composition. If not, either a smaller domain size (or component space) must be chosen, or a kinetic approach is required. More work is needed to quantify the size of the equilibration volume, and future studies should take into account the rate at which rocks “travelled through P - T space”, i.e., to link petrogenetic analysis to chronology.

PORPHYROBLAST GROWTH

Porphyroblastic growth implies a continuous supply of mineral constituents and a relatively high activation energy barrier for nucleation hence growth of existing grains is favored over formation of new nuclei. The most common example is garnet, whose unique chemical and mechanical properties can record evidence of a potentially complex path that the host rock experienced during a petrogenetic cycle (Spear et al. 1991; Vance and Mahar 1998; Caddick and Kohn 2013; Ague and Axler 2016). Though diffusion can bias the record at high temperatures (Anderson and Olimpio 1977; Tracy 1982; Caddick et al. 2010; Ganguly 2010; Kohn and Penniston-Dorland 2017, this volume), chemical zoning is commonly preserved. In metapelites for instance, garnet commonly exhibits clear compositional zoning with a systematic, bell-shaped decrease of Mn from core to rim (spessartine fraction, X_{sps} in Fig. 2a). But garnet may also provide clues about polycyclic metamorphism, where core and rim relate to two distinct metamorphic cycles (Fig. 2b). Garnet is quite resilient to mechanical and chemical weathering. In fact, metamorphic overgrowths on detrital garnet (Manzotti and Ballèvre 2013) have been recognized (Fig. 2c). Strong compositional zoning in both mono- and polycyclic garnet demonstrates its refractory nature; it does not, in general, completely re-equilibrate with the matrix during growth (Atherton 1968), though outside its stability field garnet readily interacts with hydrous fluid or melt to form secondary phases, for example,

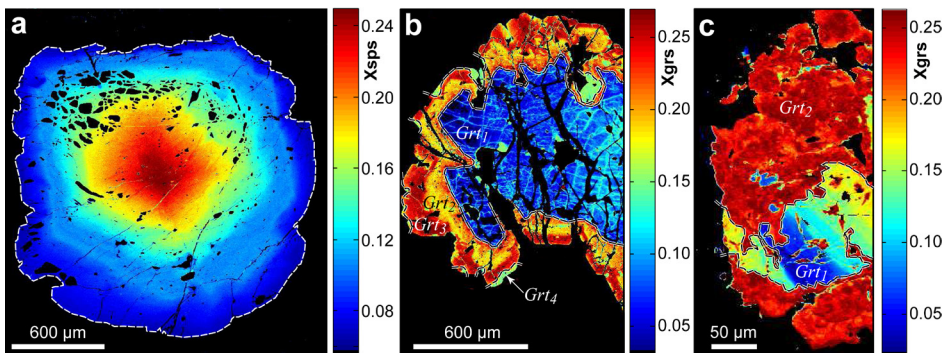


Figure 2. High-resolution end-member compositional maps of garnet grains from the Western Alps. (a) Typical bell-shaped zoning of spessartine of garnet from a metasediment of the Mont Emilius Klippe (Burn 2016); $X_{\text{sps}} = \text{Mn}/(\text{Mn} + \text{Ca} + \text{Fe} + \text{Mg})$. (b) Grossular zoning in a garnet crystal from an eclogitic micaschist of the Sesia Zone (Giuntoli 2016; Lanari et al. 2016); $X_{\text{grs}} = \text{Ca}/(\text{Mn} + \text{Ca} + \text{Fe} + \text{Mg})$. This garnet porphyroblast recorded two distinct cycles of metamorphism: a Permian LP–HT core (Grt_1) and three Upper Cretaceous (Alpine) HP–LT rims (Grt_2 , Grt_3 , Grt_4). (c) Grossular zoning in polycyclic garnet from the Zone Houillère with a LT overgrowth of spessartine-rich hydrothermal garnet (Grt_2); the core (Grt_1) is a detrital fragment that preserves pre-depositional internal zoning (Dupuis 2012).

retrograde chlorite. But where preserved, garnet serves as an archive of the P – T – X conditions of formation, as long as intracrystalline diffusion remained negligible (Spear et al. 1984; Florence and Spear 1991; Caddick et al. 2010; Kohn 2014). This fortunate ability to record and preserve chemical zoning is the main reason why garnet compositions have been so extensively used as an indicator of P – T conditions throughout its wide stability range. A method referred to as isopleth thermobarometry for garnet is based on Duhem’s theorem, which simply states that P – T conditions determine the composition and modal abundance of all phases in a closed system at equilibrium; hence the intersection of garnet isopleths for 3–4 endmember components in garnet (Fe, Mg, Ca, Mn) in P – T space indicate whether equilibrium was closely approached and, if so, under what P – T conditions. Various modeling techniques have been specially designed to be applied to garnet thermobarometry (Spear and Selverstone 1983; Spear et al. 1984, 1991; Evans 2004; Zeh 2006; Gaidies et al. 2008, 2011; Konrad-Schmolke et al. 2008; Schwarz et al. 2011; Moynihan and Pattison 2013; Vrijmoed and Hacker 2014; Lanari et al. 2017). However, determining accurate P – T conditions by modeling garnet zoning profiles demands some understanding of the interplay between chemical equilibrium (e.g., Spear and Daniel 2001; Gaidies et al. 2008), reaction kinetics (e.g., Gaidies et al. 2011; Pattison et al. 2011; Schwarz et al. 2011), and post crystallization intragranular diffusion (e.g., Ganguly et al. 1996; Caddick et al. 2010).

Several issues are separately addressed in the next paragraphs: (1) We first recall some basics of nucleation and growth. (2) Porphyroblast growth is then addressed, i.e., the successive alienation of core parts, as they typically become isolated from the reactive part of the rock, thus segregating components. In terms of the reaction volume in the matrix, this process causes and progressively enhances chemical fractionation of the reactive bulk composition. (3) The effects of fractionation on isopleth thermobarometry are then quantitatively illustrated for two examples: A pelitic schist that experienced Barrovian metamorphism (Moynihan and Pattison 2013), and a typical MORB that underwent eclogite facies transformation (Konrad-Schmolke et al. 2008). (4) Different automated strategies are currently in use to retrieve P – T information from garnet zoning based on equilibrium thermodynamics. These are presented and briefly discussed, then garnet resorption is addressed for those models. (5) Finally, the concept of distinct growth stages is reviewed based on some studies that link such metamorphic stages to age data.

Crystal nucleation and growth

Four main processes are involved in the nucleation and growth of a porphyroblast crystal: (1) Dissolution of source material provides potential nutrient material; (2) Nutrients generated at various locations and/or from different sources are transported through the intergranular medium to nucleation sites. (3) Nucleation occurs at the atomic scale where chemical species from the transport medium and possibly local reactant phases rearrange into a cluster of the product phase(s) of sufficient size to be thermodynamically stable. (4) Further precipitation onto an existing surface is termed crystal growth. The reaction interface encompasses both the detachment/dissolution at the reactant site and the attachment/precipitation of nutrients at the product site. In this conceptual model, kinetics may affect a metamorphic reaction during nucleation, during intergranular transport, and at the reaction interface. The slowest one of these three processes usually dominates the overall reaction kinetics (Pattison et al. 2011). Detachment and attachment are surface-processes whereas element transfer is a transport-process. Nucleation and growth can be affected by microstructures (favorable site model) and by reaction overstepping.

Favorable site model. Microstructural features may catalyze nucleation by increasing the local free energy, which amounts to reducing the critical energy barrier. Such is the case, for example, in crenulation hinges (Bell et al. 1986) or at grain boundaries, dislocations and cracks (Gaidies et al. 2011). Several lines of evidence support the interpretation that garnet growth is more rapid along triple-grain intersections than along boundaries separating only two grains (Spear and Daniel 2001). The heterogeneous distribution of porphyroblasts in a rock may reflect effects of the local bulk composition and/or deformation. For example, dissolution may occur along shear-dominated zones such as the crenulation limbs, whereas nucleation occurs at the crenulation hinges (Bell et al. 1986; Vernon 1989; Williams 1994). Several local processes may thus be involved in the overall transformation process leading to porphyroblast growth (Carmichael 1969).

Reaction overstepping. Even if a product phase is nominally part of the thermodynamically stable assemblage of the reaction volume, it may fail to nucleate (Waters and Lovegrove 2002). A metamorphic reaction proceeds only if and when the mechanical or chemical energy overcomes the kinetic barriers for nucleation. This delay can be viewed as a disequilibrium state required to gain the amount of energy required to initiate the interface between reactants and products that will initiate the reaction. The so-called interfacial energy (Gaidies et al. 2011 and references therein) controls the departure from equilibrium required before a phase (in our case garnet) nucleates, and the free energy of the system can attain a lower energy state. Reaction overstepping can be estimated as the difference in Gibbs free energy between the thermodynamically stable, but not yet crystallized products and the metastable reactants. This quantity is known as the reaction affinity (e.g., Fisher and Lasaga 1981; Lasaga 1986; White 2013). P - T -reaction affinity maps computed with Theriak-Domino have been used to predict metamorphic reaction overstepping (Pattison et al. 2011). Such models demonstrate, for example, that thermal overstepping may have some dependence on the heating rate (Gaidies et al. 2011; Pattison et al. 2011).

Models of equilibrium and transport control

In the framework of modeling garnet growth we distinguish two end-member models.

Equilibrium control. Chemical equilibrium is maintained at the rim of all growing phases at all times if transport rates are faster than the rates of surface processes. Equilibrium thermodynamics can be used to predict the distribution of all components among the various phases of the system. This grain boundary equilibrium model (Fig. 1b) implies that the rim composition of all the crystallizing phases will be identical and dictated by P - T conditions and other intensive variables such as fluid composition and f_{O_2} .

Transport control. If transport is the limiting factor, gradients in chemical potential are established (at least for some elements) and may evolve via the intergranular medium. Consequently, the composition of the growing phase will be controlled by the flux of these elements to the reaction interface. As thermodynamics predicts the macroscopic equilibrium state only, a kinetic description must be used to model how and how fast equilibrium will be approached at a specific reaction site.

In rocks, the attainment of chemical equilibrium and departures from it depend on scale, in both space and time. Several considerations are necessary to decide what modeling approach is most appropriate for a given situation; strong cases can be made for combining the equilibrium control and transport control approaches (e.g., Carlson et al. 2015). When the goal is to analyze and quantify petrogenesis of rock samples as a basis for detailed chronology, we regard the following considerations as essential:

- Equilibrium control may occur on different scales for different elements (Spear and Daniel 2001). Specifically, highly charged or large ions often are far less mobile than smaller or less highly charged ions (Fig. 1c).
- The concept of “chemical homogeneity” is useless beyond upper and lower spatial limits; these limits essentially depend on rock texture (e.g., layering, grain size), which evolves during petrogenesis. The spatial scale of chemical uniformity is bound to change by rock-forming processes, e.g., as a few components are sequestered by porphyroblasts or simply as static Ostwald ripening or dynamic recrystallization proceeds, by mechanical grain size reduction (grinding), or differentiation induced by plastic deformation, partial melting or metasomatic processes involving fluids.
- Trace elements contribute little in terms of the overall free energy of a rock. Equally minor is the contribution to the driving force towards equilibrium that chemical potential gradients in the trace elements may add.
- A few accessory minerals (e.g., monazite, zircon, titanite, allanite, apatite) largely sequester certain trace elements of particular interest to petrochronology. Their transport (by diffusion) is typically slow because they include large, highly charged ions, such as U^{4+} , Th^{4+} , and REE^{3+} , and they are involved in heterovalent coupled exchange mechanisms, but their mobility may be enhanced by deformation, radiation damage, and reactive fluids (e.g., Tropper et al. 2011). Modelers should be aware that accessory minerals commonly occur as relics (often armored) that appear to have metastably survived high temperatures, even partial melting.
- In general, some parts of a rock’s reaction path may be kinetically sensitive while others are not.

Taken together, these considerations indicate that sober modeling should recognize the potentials and limits of equilibrium and transport models, and possible combinations (Gaidies et al. 2011; Schwarz et al. 2011). A conceptual division of samples may be most appropriate in practice. For instance, it remains a largely open question to what extent trace element mobility will allow chemical potential gradients to be retained (or to disappear) at the temporal scale of rock-forming processes.² Reaction-driven exchanges of these trace elements between major rock-forming minerals and accessory phases, possibly mediated by fluids, may or may not be sufficient to even out concentration gradients. Current understanding of transport properties is quite insufficient for the case of highly charged minor and trace elements. The extent to which small and sparsely present grains are able to communicate deserves careful study in the future, as this promises to tighten the links between accessory mineral chronometry and petrogenetic interpretations. For example, relations between zircon equilibration and Zr-in-rutile thermometry are well documented (Meyer et al. 2011; Taylor-Jones and Powell 2015; Kohn et al. 2016).

²Note that these time scales could well be much shorter than could be resolved by mineral chronology (say $< 10^3$ – 10^5 years).

With our present goal of quantifying petrogenetic conditions, we concentrate on equilibrium control in this chapter with the assumption of local equilibrium that reduces the need to consider transport. We show that the power of thermodynamics can be enhanced and several limitations reduced by restricting the analysis to local spatial domains.

Fractionation of the reactive bulk composition during porphyroblast growth

Some component of growth zoning in garnet such as Mn are largely controlled by reactive bulk composition change generated by crystal fractionation. Mn distribution in garnet often shows a progressive decrease with a typical “bell-shaped” zoning profile from the center toward the rim (Fig. 2a, 3a). In this case the segregation of Mn during garnet growth is directly controlled by the progressive depletion of Mn in the surrounding matrix. Many studies explained such observation by a fractionation process following a Rayleigh’s (or Pfann’s) model (Hollister 1966; Atherton 1968; Cygan and Lasaga 1982; Evans 2004). Based on those results, a simple method was proposed by Evans (2004) to generate composition versus modal proportion curves for garnet. This method models the effects of the crystal fraction on the MnO content of the reactive bulk rock using the Rayleigh fractionation equation:

$$C_{\text{grt}}^{\text{MnO}} = C_{\text{bulk}}^{\text{MnO}} K_d (1 - w_{\text{grt}})^{K_d - 1} \quad (2)$$

where $C_{\text{grt}}^{\text{MnO}}$ and $C_{\text{bulk}}^{\text{MnO}}$ are the concentrations of MnO (in oxide wt%); K_d is the bulk distribution coefficient (by mass) for the element between garnet and matrix ($C_{\text{grt}}^{\text{MnO}} / C_{\text{mtx}}^{\text{MnO}}$) and w_{grt} is the mass fraction of garnet in the rock. For $K_d > 1$, the species partitions into the porphyroblast; a characteristic profile across a grain should be “bell shaped” (Fig. 3a), whereas for $K_d < 1$ the species partitions into the matrix, i.e., growing porphyroblasts are depleted relative to the matrix and show a U-shaped profile. If neither P – T conditions nor equilibrium phase relations change drastically during early garnet growth, K_d can be approximated by the ratio between $C_{\text{grt}}^{\text{MnO}}$ in the earliest garnet nucleus and $C_{\text{bulk}}^{\text{MnO}}$ (Gaidies et al. 2006). As partitioning among minerals depends on temperature, and because changes in T drive mineral growth, K_d is expected to change as the mineral grows (Hollister 1966; Kohn 2014).

To quantify the effects of fractionation of the reactive bulk composition, a case study is selected for which the prograde P – T conditions of garnet growth are well constrained. Moynihan and Pattison (2013) analyzed garnet porphyroblasts in a garnet- and staurolite-bearing schist (sample DM-06-128) from the southern Omineca belt of the Canadian Cordillera that underwent Barrovian metamorphism peaking at middle amphibolite facies during the Early Cretaceous. The evolution involved heating and burial along a linear P – T trend, followed by a heating-dominated stage accompanied first by exhumation, then renewed burial. Garnet porphyroblasts grew along a P – T path from 500 °C, 5 kbar to 570 °C, 7 kbar. From the zoning profile reported in Moynihan and Pattison (2013), we obtained a K_d value of 62 using the approximation of Gaidies et al. (2006). The corresponding MnO composition of garnet was calculated using Equation (2) and plotted against the volume percentage of garnet produced (Fig. 3c). Assuming a single population of garnet with ~5 mm diameter for a total amount of 6 vol% of garnet in the rock (as predicted by the thermodynamic model) the zoning profile matches Rayleigh fractionation with $K_d = 62 \pm 10$, reproducing to a first order the chemical zoning in MnO for this rock. In the matrix Mn is distributed between chlorite and ilmenite (Moynihan and Pattison 2013).

This technique of Evans (2004) has been successfully used in various cases to model garnet fractionation based on MnO zoning profiles (e.g., Gaidies et al. 2006; Sayab 2006; Groppo and Castelli 2010; Vitale Brovarone et al. 2011; Cheng and Cao 2015). Zoning profiles of other elements may reflect more complicated fractionation, with non-Rayleigh behavior and variable K_d during garnet growth. This is expected to occur along a P – T path that has successively involved more than one garnet-producing reactions as for most amphibolite- to upper amphibolite-facies

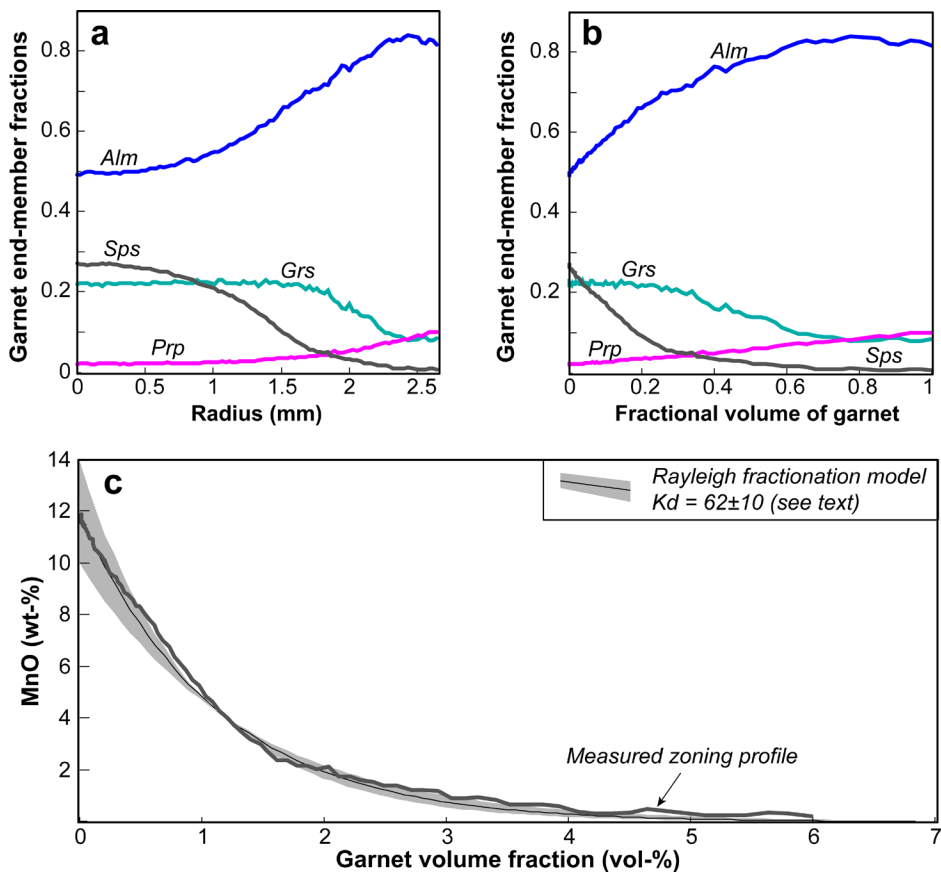


Figure 3. Garnet compositional zoning from a schist that experienced Barrovian metamorphism (modified from Moynihan and Pattison 2013) against (a) the radius, (b) the fractional volume of a single garnet porphyroblast, (c) the garnet volume fraction assuming a mode of 6 vol% garnet and a single garnet size population. The Rayleigh fractionation model for $K_d = 62 \pm 10$ is shown by the black curve in the gray domain.

rocks. For both simple and complex growth histories, quantitative models based on Gibbs free energy minimization must be favored to approximate the changes in the reactive bulk composition.

Equilibrium crystallization models vs fractional crystallization models

Two models incorporating or ignoring chemical fractionation effects during porphyroblast growth are presented and compared here. For garnet we show that (1) fractionation has a strong effect on the amount of garnet predicted, and (2) isopleth thermobarometry systematically produces erroneous P - T estimates if fractionation is ignored.

Equilibrium crystallization models (ECM). These classic models rely on isochemical P - T equilibrium phase diagrams for the given bulk rock composition and isopleth thermobarometry (Spear 1988a). Such a model cannot ‘predict’ chemical zoning because all the phases are assumed to re-equilibrate at any P - T conditions. In theory, the use of ECM models must be restricted to well-equilibrated mineral assemblages showing no relics, no chemical zoning in the mineral phases, and no partial local re-equilibration. In practice, such diagrams are often used to reveal first-order compositional and modal trends that help to interpret metamorphic mineral growth and composition changes (Kohn 2014), but the results may be inaccurate.

Fractional crystallization model (FCM). These models assume chemical fractionation of some mineral phases (usually garnet) that are produced at each step of a P – T path, where the grains produced are immediately isolated from the reactive part of the rock (Spear 1988b; Spear et al. 1991; Gaidies et al. 2008; Konrad-Schmolke et al. 2008). This is equivalent to removing the fractionating phase from the system. Step-wise growth modeling is applied, with the composition and volume fraction of the fractionating phases from the previous step(s) being isolated or removed from the reactive system.

The first major difference between FCM and ECM is the modal amount of the phase produced along a given P – T path. In their study, Konrad-Schmolke et al. (2008) documented this effect of garnet fractionation under eclogite facies conditions using a typical MORB composition. Garnet is predicted to be stable along a prograde trajectory from 525 °C, 15 kbar to 750 °C, 35 kbar using ECM (Fig. 4 in Konrad-Schmolke et al. 2008). By contrast, garnet growth ends at 650 °C and 25 kbar using FCM because the matrix is strongly depleted due to garnet fractionation (Fig. 5 in Konrad-Schmolke et al. 2008). Above that limit, garnet is no longer stable in the new reactive bulk composition. There will be a significant difference between two tectono-metamorphic scenarios based on the results from FCM and ECM models. In the present example, the FCM shows that garnet does not ‘record’ the pressure peak reached by the rock. It is important to note that the volume of garnet predicted by ECM is systematically higher than the volume predicted by FCM (Fig. 4). Accurate modeling of mineral modes along any P – T trajectory requires the use of FCM as soon as compositional zoning is observed in a sample.

To evaluate the consequences of garnet crystallization on the reactive bulk composition of typical metamorphic rocks, we again analyze the two examples of garnet growth in (1) a metapelitic schist along a typical LP–HT trajectory (Moynihan and Pattison 2013) and (2) a metabasite with a typical MORB composition along a HP–LT trajectory (Konrad-Schmolke et al. 2008). The changes in the reactive bulk rock compositions predicted using a FCM are plotted in Figure 5 against the volume percentage of garnet produced. Note that in the metapelitic schist only 6 vol% of garnet is produced along the P – T trajectory. For the metabasite, ~13 vol% is produced along the selected P – T trajectory. For the metapelitic schist, all the components

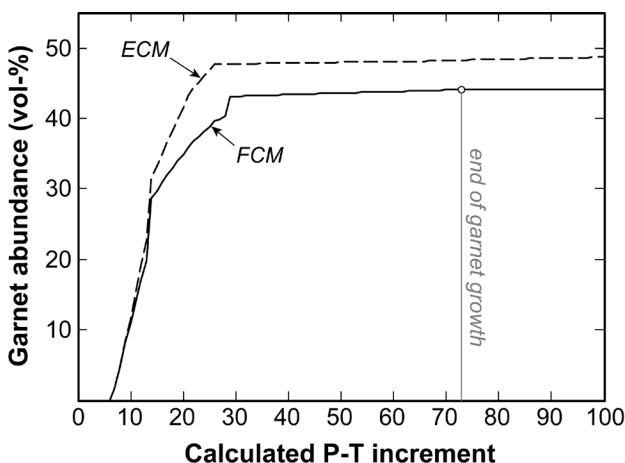


Figure 4. Volume of garnet (in vol%) predicted by ECM and FCM for a typical MORB composition along the P – T path used by Konrad-Schmolke et al. (2008). Model calculated for the system SiO_2 – Al_2O_3 – FeO – Fe_2O_3 – MgO – CaO – Na_2O using the thermodynamic dataset tc55.txt (Holland and Powell 1998), oxygen fugacity controlled by hematite-magnetite buffer.

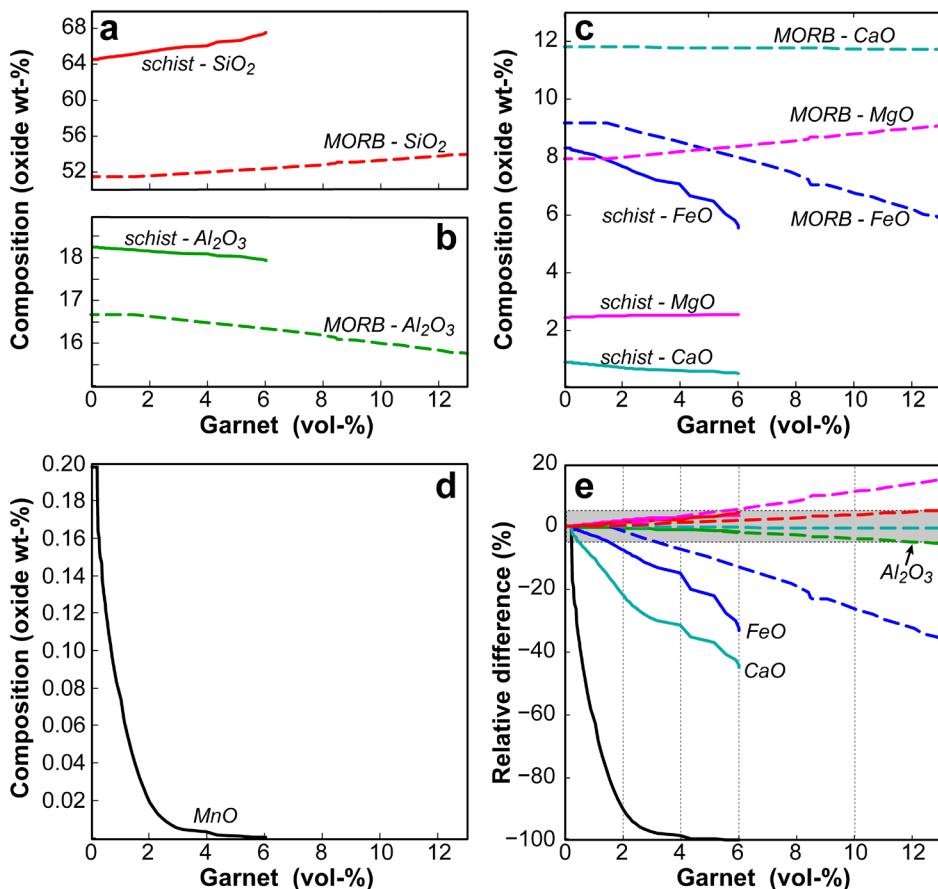


Figure 5. Evolution of the reactive bulk rock composition using a fractional crystallization model (FCM) for garnet growth in pelitic schist (Moynihan and Pattison 2013) and MORB (Konrad-Scholmeke et al. 2008) along a LP-HT and a HP-LT path, respectively. Note that along the respective P - T paths only 6 vol% of garnet is produced in the schist, whereas in meta-MORB the garnet mode reaches 40 vol% garnet (shown here to 12 vol% only, but the same trend continues). (e) Relative differences of the reactive bulk compositions to the original bulk rock composition for the two samples; note that oxides are color-coded. The gray band outlines relative differences of $< 5\%$.

(except Al_2O_3 and MgO) show significant variation during garnet growth (Fig. 5e). As previously discussed, the matrix quickly becomes depleted in MnO , i.e., the matrix loses $>90\%$ of the initial MnO once the garnet fraction reaches 2 vol%. To a lesser extent CaO and FeO decrease and finally reach 60 and 70% of their initial value once 6 vol% garnet formed. Fractionation is less pronounced for the metabasite (Fig. 5). Still, FeO and MgO are significantly affected once the garnet proportion reaches 6 vol%. From these two examples we can conclude that garnet growth systematically affects the reactive bulk composition.

What is the effect of FCM on equilibrium phase diagrams? For small fraction of garnet produced, FCM has a minor effect on the major phase relations (Zuluaga et al. 2005; Groppo et al. 2007; Moynihan and Pattison 2013). However, the compositional differences of garnet predicted stable by ECM and FCM at given P - T conditions are systematic and large enough to affect isopleth thermobarometry (Spears 1988b; Evans 2004; Gaidies et al. 2006; Chapman

et al. 2011). To evaluate this, the program GrtMod is useful because it searches the P - T conditions for which the model composition of garnet best matches the measured composition (Lanari et al. 2017), and it can be used to check differences in garnet isopleth thermobarometry between FCM and ECM model. For the schist DM-06-128 (Moynihan and Pattison 2013), this comparison was made along the original P - T path (500–650 °C, 3–12 kbar), taking three steps (at 2, 4, and 6 vol% garnet produced). Results are reported in Table 1. It is evident that ECM does not find satisfactory isopleth intersection in the P - T space for the three selected cases. In the first case (2 vol%) a ‘best match’ is found, but with a relatively high residual (Co value in Lanari et al. 2017), and it is predicted at higher pressure. Deviations are significant for almandine and grossular components (modeled: 0.74 and 0.16; measured: 0.78 and 0.14). Such deviations are due to the overestimation of CaO and FeO in the bulk rock composition, and these affect the composition of phases coexisting with garnet (Fig. 5). For the second and third cases (4 and 6 vol% of garnet), the deviations between modeled and observed compositions become even larger, i.e., they show much higher residuals. In both cases GrtMod found two distinct local minima but the lowest Co values always occur at higher pressure. Deviations of 0.10 and 0.04 are systematically observed in almandine and grossular components.

From these sensitivity tests we can conclude that FCM must always be used to model porphyroblasts growth if compositional growth zoning is observed. Note that the compositional changes become significant as soon as porphyroblasts represent >2 vol% in pelitic systems and >4 vol% in mafic systems (Fig. 5). In the following FCM are used to model growth and resorption of garnet porphyroblasts.

Table 1. Differences in P - T results between fractional crystallization models (FCM) and equilibrium crystallization model (ECM) for three stages of garnet growth (2, 4 and 6 vol% of garnet growth) along the prograde P - T path of Moynihan and Pattison (2013). Co is the residuum calculated by GrtMod. A value of Co < 0.3 generally indicates a good fit between model and measured compositions (Lanari et al. 2017).

	T (°C)	P (bar)	Co	X_{Prp}	X_{Grs}	X_{Alm}	X_{Sps}
Case 1: 2 vol% of garnet produced							
Reference	554	6916		0.055	0.141	0.779	0.024
FCM	554	6916	0.0001	0.055	0.141	0.779	0.024
ECM - S1	555	11996	0.0489	0.073	0.156	0.737	0.034
Case 2: 4 vol% of garnet produced							
Reference	571	6427		0.081	0.086	0.831	0.002
FCM	571	6427	0.0002	0.081	0.086	0.831	0.002
ECM - S1	572	11994	0.1017	0.103	0.126	0.744	0.027
ECM - S2	584	7690	0.1092	0.110	0.122	0.737	0.031
Case 3: 6 vol% of garnet produced							
Reference	583	6797		0.104	0.082	0.814	0.000
FCM	583	6797	0.0001	0.104	0.082	0.814	0.000
ECM - S1	581	11996	0.0869	0.121	0.115	0.739	0.025
ECM - S2	591	7731	0.0920	0.126	0.112	0.734	0.029

Automated fractional crystallization models designed to retrieve P - T paths from chemical zoning

Examples of simplified fractionation modeling based on BSE or X-ray images and electron microprobe analyses can be found in many studies (e.g., Marmo et al. 2002; Tinkham and Ghent 2005a; Zuluaga et al. 2005; Zeh 2006; Caddick et al. 2007). Four methods presented here are based on forward equilibrium models and require no manual alteration of the reactive bulk composition to account for material sequestered in garnet crystal cores.

- The first automated method models garnet zoning and the composition of coexisting phases along an arbitrarily selected P - T path using Gibbs free energy minimization. The generated compositional profiles are then compared against data along high-resolution zoning profiles analyzed by electron microprobe (Konrad-Schmolke et al. 2008; Hoschek 2013; Robyr et al. 2014). These models merely test if the chosen P - T trajectory is in accordance with the observed zoning (or vice versa). In fact, the three studies cited found some mismatch between model compositions and observed zoning profiles, in some cases with systematic and large discrepancies (>0.08 in the end-member proportions). Is the P - T trajectory at fault or the assumption of grain boundary equilibrium? The two following approaches aim to derive the optimal P - T trajectory and proposed numerical methods to improve its selection.
- Moynihan and Pattison (2013) provide a MATLAB[®]-based program linked to Theriak (de Capitani and Brown 1987; de Capitani and Petrakakis 2010) that uses an inverse modeling strategy to derive the “best” P - T trajectory by minimizing a misfit parameter, i.e., the weighted differences between measured and model compositions. For any garnet spot analysis, the best P - T conditions are found by matching the model against the measured composition, and the procedure is successively applied to all analyzed points from core to rim. Using this approach, Moynihan and Pattison (2013) successfully modeled the observed zoning profile (see their Fig. 6a). The match is excellent and demonstrates that in favorable cases, equilibrium thermodynamics in the context of fractional crystallization can be successfully used to model porphyroblast growth, provided the P - T path is part of the model optimization.
- Similarly, Vrijmoed and Hacker (2014) provided a MATLAB[®]-script linked to Perple_X (Connolly 1990, 2005). It uses a brute-force inverse computational method to determine the best P - T trajectory by minimizing the differences between predicted and the entire measured garnet compositional profiles along different trajectories. This routine examines a multitude of paths from an unspecified starting P - T to a predetermined maximum P - T point. The best match is selected such that all endmember mole fractions of the fractionated garnet show least discrepancy between data and model. Several tests based on published zoning profiles data show that brute force can pay off.
- Finally, a fourth approach is of interest: Program Theria_G (Gaidies et al. 2008) allows the simulation of porphyroblast nucleation and growth using a FCM for any given P - T trajectory, and it takes into account further possible modifications driven by intragranular multi-component diffusion. Theria_G uses the Gibbs free energy minimization routine of Theriak and simulates the formation of a garnet population with variable grain size that can be compared with observations. The P - T trajectory can also be part of the model optimization as shown by Moynihan and Pattison (2013).

Crystal resorption and implications on fractional crystallization models

The models presented above take into account the fractionation due to garnet growth and how this affects the reactive bulk composition. However, garnet may also be affected by local resorption (de Béthune et al. 1975; Kohn and Spear 2000; Ague and Axler 2016), in some extreme cases leading to atoll or mushroom garnets (Cheng et al. 2007; Faryad et al. 2010;

Roby et al. 2014). More commonly, the production of staurolite and biotite at the expense of garnet and chlorite causes the resorption of garnet and a step in the zoning profile (Spear 1991). Garnet resorption has been invoked to explain the peripheral increase in MnO (dubbed near-rim kick-up) observed in some grains. Typically this results from partial consumption or dissolution of garnet crystals during cooling and exhumation, which returns Mn to the reactive matrix (Kohn and Spear 2000), and Mn can show retrodiffusion features in garnet (de Béthune et al. 1975). The amount of Mn in the near-rim kick-up has been used as a semi-quantitative measure of the volume of garnet dissolved. Kohn and Spear (2000) estimated that 45% of garnet was dissolved in an amphibolite facies metapelite from the central Himalaya of Nepal. Based on forward equilibrium models (see below) and different types of evidence Lanari et al. (2017) estimated that 50% of garnet in eclogitic micaschist was dissolved during HP metamorphism before a new episode of garnet growth. As shown above garnet chemical fractionation has a strong impact on the reactive bulk composition. Fractional crystallization drives the reactive bulk composition away from the garnet composition. Thus, resorption of garnet drives the reactive bulk composition back towards the garnet composition.

The effects of garnet resorption on forward equilibrium models were investigated by Lanari et al. (2017), who proposed a numerical strategy and a MATLAB[®]-based program (GrtMod) linked to Theriak. It allows numerical simulation of the evolution of garnet based on compositions of successive growth zones, optimization of successive local reactive bulk compositions, accommodating resorption and/or fractionation of previously crystallized garnet. Each growth stage here is defined as an interval during which garnet grows at fixed P - T - X conditions while in equilibrium with the same stable matrix assemblage. This approach uses compositional maps (instead of profiles) to define the growth zones and to estimate average compositions.

Timing of porphyroblast growth

In porphyroblast petrochronology, two different ways are generally used to link metamorphic age (t) with temperature and pressure: (1) in-situ dating of the porphyroblast or (2) textural correlation between the porphyroblast and dateable accessory minerals either trapped as inclusions or chemically correlated to distinct zones within a porphyroblast (e.g., Pyle and Spear 1999; Regis et al. 2014).

In situ dating of garnet porphyroblasts is the most attractive method to constrain the time interval of growth because porphyroblasts commonly contain inclusions that help constrain P - T , as can the chemical zones that recorded successive growth stages. Several potentially useful isotopic systems (Sm-Nd, Rb-Sr, Lu-Hf) are extensively discussed in Baxter et al. (2017, this volume). Rb-Sr dating of garnet is restricted to a few cases because it is not always realistic to assume that the whole-rock or matrix compositions adequately reflect the reactive bulk composition at the time garnet grew (Sousa et al. 2013). Sm-Nd is most commonly used because Sm and Nd generally are uniformly distributed in garnet (Kohn 2009), whereas Lu and Hf may be restricted towards early garnet growth (because Lu strongly fractionates into the core, depleting the matrix in Lu). In addition, much more material is required per analysis to obtain ages of specific zones using Lu/Hf. Sm/Nd is most powerful for dating specific garnet zones (e.g., Pollington and Baxter 2010), since improved analytical techniques now permit analysis of very small volumes (Harvey and Baxter 2009; Dragovic et al. 2012), such as single growth zones mapped by electron microprobe (Gatewood et al. 2015). Ages are calculated based on isochrons for each garnet zone and the surrounding matrix, and such ages rest on assumptions about the extent of trace element homogenization.

Instead of applying direct garnet dating many studies have used textural correlations between the porphyroblast and dateable accessory minerals trapped as inclusions. An example of monazite is presented in the following paragraphs. Other examples are given in Williams et al. (2017, this volume).

Textural correlation is conceptually simple (e.g., Kohn 2016) and obviously requires in situ dating of accessory phases to preserve textural relations. In particular, U–Th–Pb dating of monazite has become one of the primary tools for constraining the timing of moderate to high-grade metamorphism (Harrison et al. 2002). Of course, the youngest inclusions only set an upper age limit to the enclosing garnet growth zone. If an accessory formed just before it got trapped in a growing porphyroblast, it presumably was isolated from the matrix and thus protected from later re-equilibration, recrystallization or overgrowth. Such an (idealized) scenario should generate an age gradient among inclusions from the core of the porphyroblast to its rim.

Examples. Mottram et al. (2015) dated monazite included in garnet from pelitic schist of the Lesser Himalayan Sequence. Monazite trapped in garnet cores gave (common-Pb and Th-corrected) $^{238}\text{U}/^{206}\text{Pb}$ ages of 20.7 ± 2.2 Ma (from 4 single-spot analyses), inclusions in the mantle surrounding the core show ages of 17.9 ± 0.5 Ma (3 analyses), and inclusions in the rim 15.8 ± 1 Ma (4 analyses). Three distinct stages of garnet growth with different inclusion patterns are visible in chemical maps. As xenotime was absent in this sample, one might expect monazite dissolution during garnet growth (Spear and Pyle 2010). The process invoked by Mottram et al. (2015) assumes that monazite grains present in the matrix underwent continuous and complete re-equilibration during garnet growth. However, it is not clear by what process such re-equilibration happened nor whether there merely has been overgrowth. Inclusions trapped by the growing garnet were shielded, since diffusion of U, Th and Pb in garnet is slow. Many other studies have reported evidence that garnet porphyroblasts provided such shielding and found monazite inclusions trapped in garnet porphyroblasts to be older than in the matrix (Foster et al. 2000, 2004; Martin et al. 2007; Hoisch et al. 2008). Yet, to derive robust estimates on the time and tempo of garnet growth, careful documentation of the inclusion location is required, e.g., reporting the distance of the inclusion from the core (in equatorial sections). In addition, inclusions that seem connected to the matrix by hairline fractures or microcracks must be avoided, as these may have been subject to interaction with the matrix or re-equilibration (Montel et al. 2000; Martin et al. 2007). For instance, Martin et al. (2007) compiled 196 in situ Th–Pb dates of monazite inclusions obtained by LA-ICP-MS and found that microcracks allowed communication between the interior of the garnet and the matrix, facilitating dissolution, recrystallization, and intergrowth formation.

Assuming that continuous re-equilibration of matrix monazite does happen, as suggested by Mottram et al. (2015), is it the rule or the exception? Some studies have indicated incomplete re-equilibration to interpret the observed age distribution. For instance, monazite ages in a garnet–biotite schist from Bhagirathi valley in Garhwal Himalaya (Foster et al. 2000) range between 40 and 25 Ma. The age of monazite *m1* included in garnet cores is ~ 39.5 Ma, whereas monazite *m2* in garnet rims spread in age between 36 and 41 Ma (Fig. 6). However, instead of invoking partial re-equilibration, we contend that the data indicate partial dissolution of *m1*-monazite, and discrete overgrowth by *m2*. In the matrix, no *m1* and only one survivor of *m2* was found (Fig. 6), suggesting strong dissolution of monazite *m1* and *m2* before the formation of a new generation *m3* at 30–27 Ma. So, we suggest partial replacement rather than “re-equilibration”. To ascertain whether this (or some alternative) process was responsible for monazite growth, geochemical tracers for monazite should be analyzed, and readily interpretable ones are available: Th and Y contents and their zoning (Kohn et al. 2005; Williams et al. 2017, this volume) are most helpful.

A model of partial replacement is also supported by the comprehensive dataset of spatially distributed ages reported by Hoisch et al. (2008). Monazite inclusions were dated (SIMS, Th–Pb) in several garnet grains from upper amphibolite facies pelitic schist in the northern Grouse Creek Mountains, Utah. Compositional maps exhibit three successive growth zones with distinct

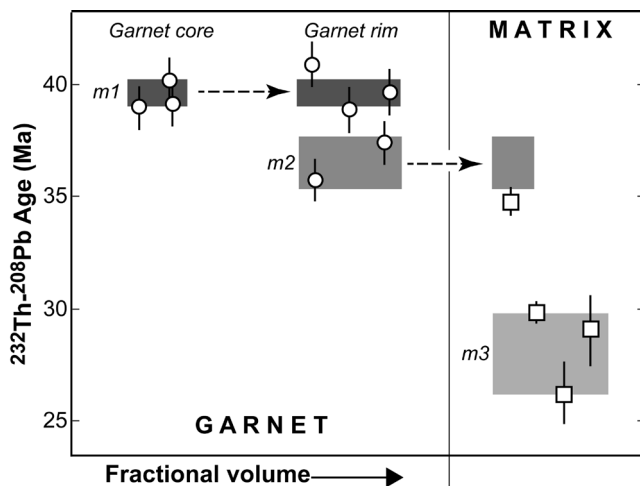


Figure 6. Monazite ages from grains trapped as inclusions in garnet (circles) and grains in the matrix (squares) of a biotite schist from Bhagirathi valley, Garhwal Himalaya (modified after Foster et al. 2000).

compositions from a core to a mantle and a rim (inset in Fig. 7a). The age of inclusions from different grains (*gm1b-e* and *gm3h*) correlated with chemical zoning in the three zones, as shown in plots against the fractional garnet volume (Fig. 7). Ages generally decrease toward garnet rims, and Hoisch et al. (2008) interpreted the monazite ages as decreasing linearly with increasing mode (volume) of garnet. Kohn (2016) pointed out that this interpretation implies that analytical errors were underestimated. Certainly the monazite inclusion ages in the three growth zones show scatter beyond the analytical error (Fig. 7a). An alternative interpretation is to regard each inclusion age as a maximum age estimate of a single growth stage (Fig. 7b). Thus partial preservation of older monazite ages in discrete, successive growth zones is visible and suggestive of a process of incomplete and continuous replacement of monazite, along the lines previously discussed.

Is partial or complete replacement the only process to explain the age trend recorded by monazite inclusions? Monazite textures give some indications: Grains from a sillimanite-bearing metapelite from the Hunza Valley in Pakistan studied by Foster et al. (2004) exhibit complex zoning patterns with four distinct growth zones (Fig. 8), suggesting a succession of partial resorption and precipitation stages. Monazite *m1* grew slightly prior to garnet and was then partially dissolved during growth of the garnet core (Fig. 8). Monazite *m2* grew after the garnet core and was then captured as inclusions in garnet rims. The enrichment in Y found in rim garnet was interpreted as the prograde breakdown or consumption of xenotime (Fig. 8). Because monazite *m3* is not observed as inclusions in garnet, it is likely that it grew coevally with xenotime during the garnet resorption stage. Finally the last monazite *m4* grew locally in the matrix, in equilibrium with xenotime. Some monazite grains in the matrix exhibit the four growth zones, but with clear resorption features separating them. The preservation of several growth zones of monazite in this sample is well supported by both textures and chemical zoning (Fig. 8). Resorption of monazite appears to be correlated to garnet growth and provides some constraints on timing. Based on the textural relationships (Fig. 8), we can conclude that the garnet core grew between 80 and 68Ma and garnet rims between 60 and 58Ma. A break of 8Ma occurred between the two stages of growth of garnet (core and rim). This dataset with its extensive documentation of the textural and chemical relationships also provided a fairly precise estimate ($2.4 \pm 1.2^\circ\text{C}/\text{Ma}$) of the heating rate experienced by the sample (Foster et al. 2004).

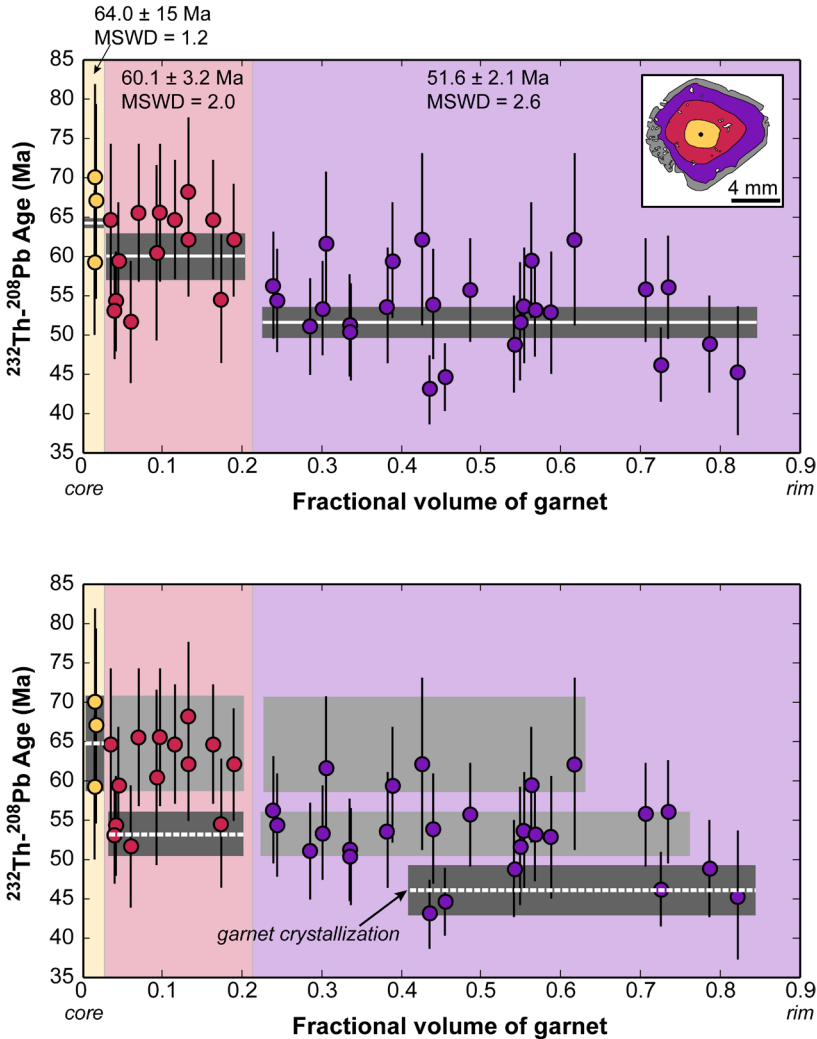


Figure 7. Ages from monazite inclusions (2σ) trapped in three garnet crystals (*gm1b*, *gm3h*, *gm1e*) from upper amphibolite facies pelitic schist in the northern Grouse Creek Mountains, Utah plotted against the fractional volume of garnet (modified after Hoisch et al. 2008). The garnet crystals were divided into three successive growth zones (see inset); ages are plotted in corresponding colors. (a) Average age and weighted uncertainty of inclusion ages from the three growth zones. (b) Alternative interpretation of the age distribution, assuming partial re-equilibration of monazite grains during growth or overgrowth.

Any petrochronological interpretation demands good documentation of both inclusion texture and chemical zoning. From the selected examples of textural correlation, several main conclusions can be drawn: (1) Age patterns can be complex because of partial replacement (for example, by dissolution–reprecipitation, Putnis 2009; Grand’Homme et al. 2016). (2) P – T modeling based on the concept of FCM is required, incorporating an inverse numerical strategy to obtain the most likely P – T trajectory (Moynihan and Pattison 2013; Vrijmoed and Hacker 2014; Lanari et al. 2017). This is the price to be paid if we want to obtain robust P – T – t estimates for successive growth zones. If, in addition, inclusion ages are combined with host (here garnet) dating, this adds certainty, especially to the significance of the earliest inclusion age.

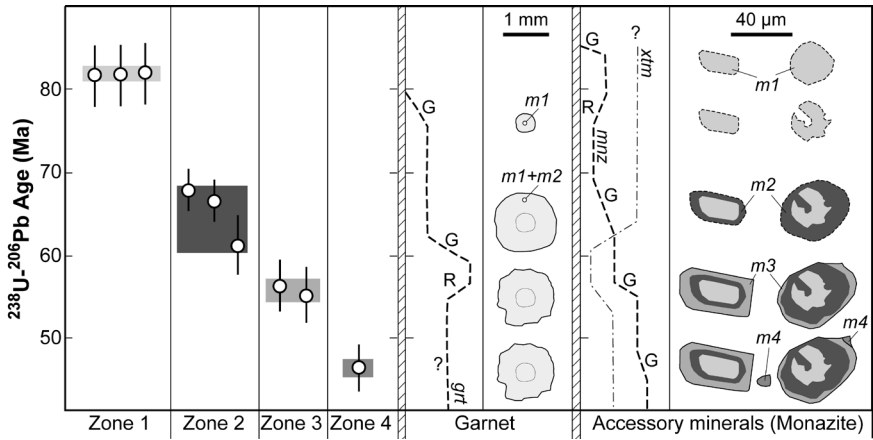


Figure 8. Monazite petrochronology on inclusions and matrix grains from a sillimanite bearing metapelite from the Hunza Valley in Pakistan (modified after Foster et al. 2004). The ages are reported together with schematic volume fractions of garnet, monazite, and xenotime through time and the corresponding textures. Abbreviations: G, growth; R, resorption, mnz, monazite; xtm, xenotime; grt, garnet. The four monazite zones ($m1 \dots m4$) correspond to the different generations discussed by Foster et al. (2004).

BULK ROCK COMPOSITION EFFECTS ON MELT PRODUCTION AND ACCESSORY MINERALS

Many studies have pointed out the strong effect bulk rock composition has on major and accessory mineral stability and on melt production (e.g., Spear 1993; Stevens et al. 1997; Pickering-Witter and Johnston 2000; Tinkham et al. 2001; Evans and Bickle 2005; Janots et al. 2008; Kelsey and Hand 2015; Yakymchuk et al. 2017, this volume; Zack and Kooijman 2017, this volume). To illustrate this effect in a petrochronological framework, we present two case studies of the regional metamorphic aureole in the Mt Stafford area, central Australia. A metamorphic field gradient from low-pressure greenschist- to granulite-facies is exposed, and Greenfield et al. (1996) divided the terrain into five metamorphic zones (Fig. 9a). The Proterozoic metasedimentary rocks of the Mt Stafford area comprise aluminous metapelites interbedded with metapsammite layers and cordierite or amphibolite granofels on a centimeter to meter scale. In the migmatite zones the interbedded metapelite and metapsammite form bedded migmatites preserving sedimentary features (Greenfield et al. 1996) that suggest in situ melting (caused by a series of biotite breakdown reactions) without substantial migration of melt (Vernon and Collins 1988). Bulk rock compositions are constant across the various zones (Greenfield et al. 1996), confirming the absence of significant melt mobilization. This result was essential to use the bulk rock composition as representative of the equilibration volume. Based on this assumption, White et al. (2003) reconstructed the melt production history across the successive zones (Fig. 9b) using equilibrium phase diagrams computed for the bulk rock compositions of Greenfield (1997). Metapelite produced more melt at lower temperatures, whereas metapsammite experienced additional major melt-production at higher temperatures (zone 5 in Fig. 9). This example shows the control of the bulk rock composition on the melt production history. It is important to note that this approach would not work in case of large-scale melt migration that would change the reactive bulk composition.³

³ In such cases a melt extraction step could be added in modeling along a P - T loop. For example, 6 vol% of melt could be extracted once the proportion reaches the melt connectivity transition at 7 vol%, and a new reactive bulk composition would be calculated for use in the next steps.

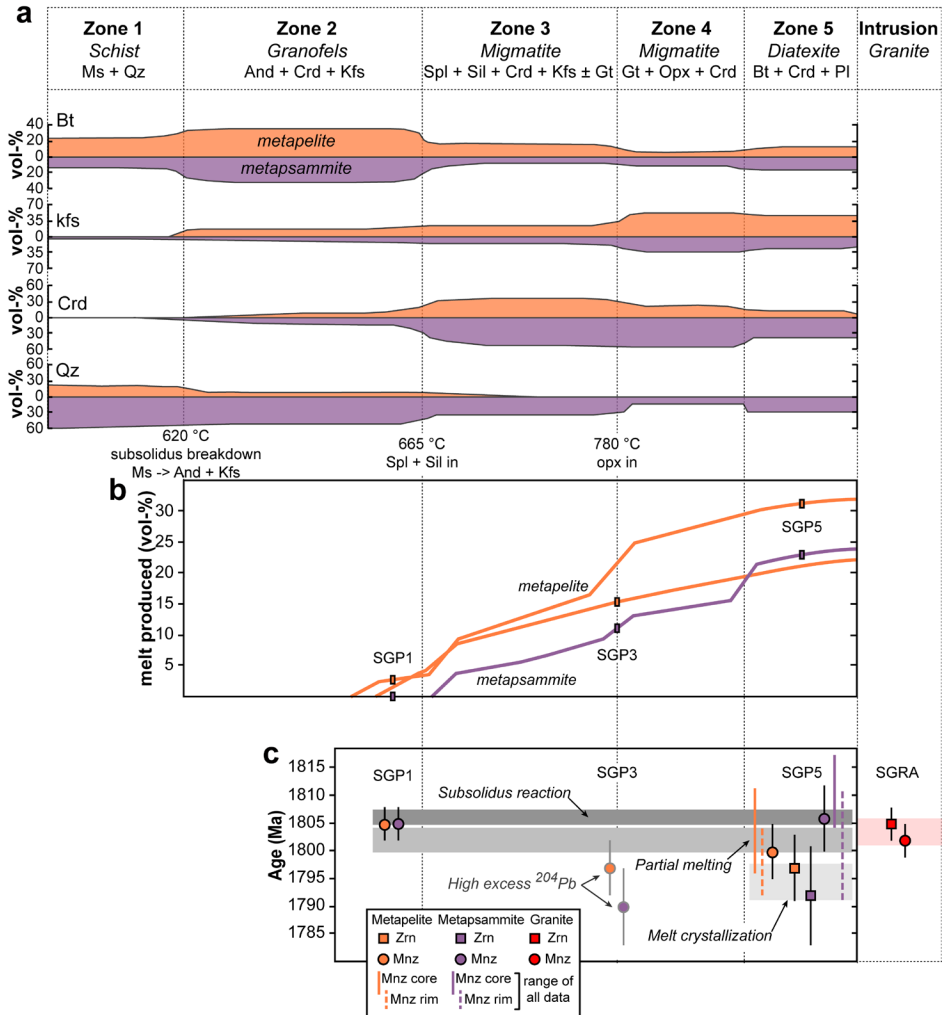


Figure 9. Petrochronological investigation of a metamorphic aureole from the Mt Stafford area in central Australia. (a) Metamorphic zones and mineral modes from Greenfield et al. (1996). (b) Melt fractions for two metapelite and one metapsammite samples from White et al. (2003). Sample numbers refer to those with age data for accessory phases (Rubatto et al. 2006). (c) Ages of monazite and zircon. Dates for SGP3 are not considered here because of possible excess ^{204}Pb , as discussed by Rubatto et al. (2006).

Taking the scenario and quantification of the melt history from White et al. (2003), age data (Rubatto et al. 2006) for these same rocks can be put into context. The metamorphic behavior of monazite and zircon depends on host-rock composition (Wing et al. 2003; Fitzsimons et al. 2005; Rubatto 2017, this volume), and metapelites and metapsammites affect inherited zircon and monazite in different ways. In the case of the Mt Stafford aureole, monazite cores show a less pronounced Eu anomaly than the rims, and both are interpreted as due to prograde growth, with the amount of coexisting potassic feldspar increasing (Rubatto et al. 2006). In the higher-grade samples, monazite rims may have formed later, as they show an increase in Gd/Lu, which reflects strong fractionation of Lu into garnet cores. Therefore, the monazite

rims most likely grew during a limited period of garnet resorption close to peak metamorphic conditions. This scenario is supported by the compositional zoning of garnet that exhibits clear evidence of core resorption (Rubatto et al. 2006). Trace element maps (Th and Y) of the last monazite growth zone would help in interpreting how the last monazite formed. However, the solubility of monazite as well as the melt volume increase with temperature (Montel 1993; Stepanov et al. 2012), one would expect resorption not growth (Kelsey et al. 2008). Chemical characterization of monazite—ideally based on compositional maps (Mahan et al. 2006; Williams et al. 2007, 2017, this volume)—is best done prior to chronological microanalysis (Kohn et al. 2005). Other studies have reported that monazite rims may also form during cooling from crystallizing melt (Pyle and Spear 2003; Kohn et al. 2004; Johnson et al. 2015).

In migmatites and residual granulites new metamorphic growth of zircon occurs because the concentration of Zr and light rare earth elements (LREE) increases in the melt during cooling (Kohn et al. 2015). The corresponding age data thus reflect high-temperature retrogression (Roberts and Finger 1997; Whitehouse and Platt 2003; Kelsey and Powell 2011; Yakymchuk and Brown 2014; Kohn et al. 2015), and indeed zircon ages from the Mt Stafford aureole are slightly younger than monazite ages (Fig. 9c), supporting growth upon cooling and melt crystallization.

In this set of samples, we observe that (1) the ages between monazite (core and rim) and zircon are slightly different, and (2) a systematic shift occurs between the weighted mean ages of accessory minerals from higher-grade samples of metapsammitic versus metapelitic compositions. For instance, monazite ages in the former are slightly older than those in the latter (Fig. 9), though this shift in age is almost within analytical error. The apparent age differences are most likely due to migmatites reaching the solidus at different temperatures for the different local bulk rock compositions (Yakymchuk and Brown 2014). This example can be used to demonstrate that if chemical and age differences do exist between two metasedimentary layers with different bulk rock compositions, successive P - T - t investigations should be made for the distinct layers. The same applies to distinct domains occurring within a single layer, but in the case of Mt Stafford these have not been investigated. Implications for domainal rocks are discussed in the next section.

LOCAL REACTIONS AND FORMATION OF DOMAINAL ROCKS

Chemical differentiation processes are essential to the formation of many metamorphic rocks (e.g., schist, hornfels, banded gneiss, migmatite). While differentiation occurs at various spatial scales, we focus here on evidence in single rock specimens and on processes that lead to chemical segregation in these, thus producing compositional domains. Once more, our goal is essentially to “read rocks”, i.e., to understand samples petrogenetically and quantify the conditions at which they formed. We showed above that models rooted in chemical thermodynamics remain powerful, if they are cleverly applied to analyze rocks that have not experienced strong chemical differentiation (e.g., melt loss) or chemical segregation (zoned porphyroblasts). In general, complexity levels increase if we consider rocks with textural and chemical heterogeneity—both commonly evident in interesting samples. Clearly such rocks did not reach anything like rock-wide chemical equilibrium, but documenting local domains allows us to investigate them and paves the way to understand their petrogenesis.

In this section we examine further evidence for and consequences of domain formation from various rock types. Touching briefly on isolated segregations, such as corona structures or pseudomorphs after porphyroblasts, we mostly concentrate on analyzing spatially more extensive and organized domains, such as typically occur in migmatites.

Evidence of local reactions in discrete textural domains

Domain formation requires an initial step of physical segregation of material (DeVore 1955) to create spatial heterogeneity in composition. Such initial heterogeneity may form, for example, by mass transfer during a period of interaction with a reactive fluid (e.g., Beinlich et al. 2010) or by metamorphic differentiation (Fletcher 1977; Foster 1981, 1999), enhanced by solid-state transformations (e.g., Brouwer and Engi 2005; Lanari et al. 2013), deformation (e.g., Mahan et al. 2006; Goncalves et al. 2012; López-Carmona et al. 2014), or partial melting (Milord et al. 2001; Kriegsman and Nyström 2003).

As shown above, prograde growth of garnet porphyroblasts generates strong local heterogeneity in the rock composition, and this effect is not limited to garnet; indeed it may be even more pronounced for porphyroblastic lawsonite or kyanite if they are later involved as reactants in replacement reactions. Such reactions may respond to these unusually Ca- and Al-rich domains, which are commonly identified because they preserve the original shape of the porphyroblast (as pseudomorphs), and they generate new mineral assemblages very distinct from the rest of the rock matrix (Carmichael 1969; Selverstone and Spear 1985; Foster 1986; Carlson and Johnson 1991; Elvevold and Gilotti 2000; Ballevre et al. 2003; Brouwer and Engi 2005; Zhang et al. 2009; Verdecchia et al. 2013; López-Carmona et al. 2014). In some cases, such domains can be modeled as a closed system. For example, Brouwer and Engi (2005) combined backscatter electron images with electron microprobe spot analyses to obtain local bulk compositions of four domains in retrogressed kyanite-bearing eclogite from the Central Swiss Alps. The models account for the development of plagioclase symplectites involving very Al-rich phases like corundum, hercynite, and staurolite, which are not normally expected in rocks of basaltic bulk composition. This technique can be generalized to any textural domain for which the local bulk compositions are calculated from mineral compositions and estimated mineral modes (Tóth et al. 2000; Korhonen and Stout 2005; Mahan et al. 2006; Riel and Lanari 2015; Cenko-Tok et al. 2016; Guevara and Caddick 2016) assuming limited chemical interaction among the domains (see below). In delimiting domains, a certain amount of judgment is needed, and some assumptions are implied (Elvevold and Gilotti 2000; Kelsey and Hand 2015).

Fluid influx can cause metamorphic differentiation as well, and it may lead to significant changes in the local reactive composition (Putnis and John 2010). Using an example from the subduction complex of the Tianshan mountains (China), Beinlich et al. (2010) reported the transitional conversion from blueschist to eclogite accompanied by a change in composition (from Ca-poor to Ca-rich) along a profile sampled perpendicular to a vein (10–15 cm thick). Equilibrium phase diagrams computed for the two distinct bulk rock compositions indicate that both mineral assemblages were stable at the same peak P – T conditions (21 ± 1.5 kbar and 510 ± 30 °C). Here the fluid affected the local composition and probably played a significant role to achieve chemical equilibrium. However, it has long been debated (e.g., Ridley 1984) why blueschists and (low-temperature) eclogites coexist in some areas; differences in bulk composition (Brovarone et al. 2011) or in P – T conditions (Davis and Whitney 2006) may be responsible.

The presence of textural domains and compositional differences among these may or may not imply chemical potential gradients. If chemical exchange between domains was very inefficient, each domain may be regarded as essentially a closed system, and thermodynamic modeling poses no problem. If transport was very limited for only a few chemical components (e.g., of trace elements), but efficient for the others, then chemical potential gradients between domains may have been essentially zero for most components, i.e., (partial) equilibrium was maintained between the domains. However, wherever local mineral assemblages within textural domains indicate substantial chemical potential gradients between them, transport (of these components) between the domains evidently happened, but at rates too low to attain overall equilibrium.

Chemical potential gradients and element transfer between domains

If two systems A and B are in thermal equilibrium and are open with regard to a mobile component i , then μ_i must be the same in both systems, otherwise there is a tendency for transfer of i between the two systems. When such a distribution has been attained, the free energy of the total system is at minimum with regard to the distribution of component i (Thompson 1955). This model of mobile component has been termed selective chemical interaction. An example of this principle concerns migmatites, which are domainal rocks with a leucosome and a melt-depleted melanosome (here considered a residue). The segregation of solids and melt and the subsequent evolution of their mineral assemblages can be modeled using T - X residue–melt equilibrium phase diagrams (White et al. 2001), these are binary diagrams displaying the evolution of the phase assemblage for reactive bulk composition lying between a residue (melanosome or restite) and a melt-rich domain (leucosome). Of interest here is the role that diffusion of H_2O can play between leucosome and residue in the crystallization history of (segregated) melt in contact with the residue. If the physical separation of melt from its residue is purely mechanical and happens at chemical equilibrium, there are no gradients in chemical potential. However, subsequent cooling results in chemical re-equilibration of now separate domains of different reactive bulk compositions. Now chemical potential gradients will be established, in particular $\mu(H_2O)$ will rise upon crystallization of the melt-rich domain. Where in contact with restite, equilibration between the two domains requires diffusion of H_2O from the leucosome to the melanosome. White and Powell (2010) used this model of selective chemical interaction to show that the diffusive interaction of H_2O between residue and segregated melt—aiming to equalize $\mu(H_2O)$ —promotes the crystallization of anhydrous quartzofeldspathic products in the leucosome and hydration of the residue. Further studies are warranted to identify evidence of interaction for other elements between the two domains, possibly with different length scales. It is crucial to understand such scales if equilibrium thermodynamics (based on local bulk composition, see below) may be applied or not.

Chemical potential gradient within domains

Frozen-in chemical potential gradients can also be observed within single domains provided that diffusion-controlled structures such as coronae are preserved. An interesting approach based on equilibrium thermodynamics and quantitative chemical potential diagrams has been proposed by White et al. (2008) who reconstruct the chemical potential gradients preserved in the final corona structure. The same approach was applied by Schorn and Diener (2016) to investigate coronae developed at the expense of magmatic plagioclase and orthopyroxene during the gabbro-to-eclogite transformation. So far, such models are restricted to simple systems with some general assumptions on components in excess or assumed to be immobile.

Size of the equilibrium volume versus scale of the model

As discussed earlier, the size of the equilibrium volume is controlled by the diffusion rate of the elements in the intergranular medium. Knowing diffusion rates is essential as they may set a spatial limit within which rocks can maintain global chemical equilibrium as they evolve. Because experimental data are sparse or may not apply, few reliable estimates on rates of intergranular diffusion are as yet available; they have instead been extracted from natural examples (Carlson 2002 and references therein). Because it is difficult to constrain the duration of intergranular diffusion tightly, these rates are not very well known, but Carlson (2010) succeeded in estimating the rate of intergranular diffusion of Al and its dependence on temperature for H_2O -saturated and fluid-undersaturated media (Fig. 10). Data for Al diffusion are essential because many studies found the diffusive transport of Al to exercise the dominant control on overall rates of reaction for aluminosilicates (Carmichael 1969; Foster 1977, 1981, 1983; Carlson 1989, 2002, 2010; White et al. 2008). To the extent that this may apply, the diagram in Figure 10 sets limits on the length scales over which reactions and

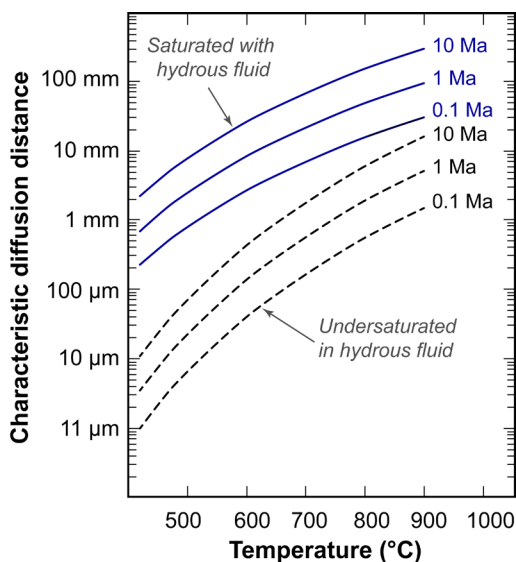


Figure 10. Characteristic intergranular diffusion length scale for Al in a medium saturated in hydrous fluid (blue curves) and undersaturated in fluid (black dashed curves); modified from Carlson (2010).

chemical equilibration can be expected for a range of temperature and typical duration of metamorphic transformations. For example, the data indicate that at upper amphibolite facies conditions (say 600–700 °C), domains 0.5 mm apart will require 1 Ma to equilibrate if grain boundaries are not fluid-saturated, whereas domains 5 mm apart should equilibrate in 100 ka when saturated with hydrous fluid. But do fluids ever persist that long?

In any case, this sort of analysis may serve to indicate whether we may rely on chemical equilibrium models to infer petrogenetic conditions from domainal rocks. Where valid, it is useful to analyze P - X or T - X phase diagrams, calculated for a range in local bulk rock compositions ($X_1 \dots X_2$), corresponding to different domains. Individual textural domains can be analyzed to determine the local bulk compositions (Tóth et al. 2000; Brouwer and Engi 2005; Riel and Lanari 2015; Cenki-Tok et al. 2016) and then the equilibrium assumption can be tested by comparing predictions from forward thermodynamic models against observed phase relations. To support such comparisons, we propose an analytical method to quantify variations in the local bulk composition based on standardized X -ray maps.

QUANTITATIVE MAPPING OF THE LOCAL BULK COMPOSITION AS A BASIS FOR MODELING

It is possible to correct for the effects of chemical fractionation and chemical differentiation described in the previous sections using quantitative compositional maps (expressed in oxide wt%) and to extract local compositions from such a map. The first application (to our knowledge) that used quantitative compositional maps to obtain the local bulk composition was published by Marmo et al. (2002) who focused on two eclogite samples showing zoned garnet porphyroblasts. The authors examined the effect of garnet core and mantle fractionation on the bulk rock composition using compositional maps with a standardization based on the semi-empirical Bence and Albee (1968) matrix correction algorithm (Clarke et al. 2001). Major progress since then involved a density correction, clarifications on the choice of domain boundaries, and a correct extrapolation from 2D to 3D. This last point is tricky; for example it is easy to overestimate the contribution of garnet cores, as surface fractions need to be properly converted to volume fractions, but equally easy to underestimate cores—simply by mapping a grain sectioned off-center.

The influence of various assumptions on the local bulk composition estimates is shown below, but an adequate mapping strategy is definitely required to produce high-quality standardized maps.

Quantitative X-ray mapping

Since the first X-ray “spot maps” measured using an electron probe micro-analyzer (Cosslett and Duncumb 1956), both the instruments and techniques have been greatly improved. Although quantitative methods (Kohn and Spear 2000; Clarke et al. 2001; De Andrade et al. 2006) and computer programs (Tinkham and Ghent 2005b; Lanari et al. 2014c) are available to obtain oxide wt% maps, many studies still combine uncorrected ‘semi-quantitative’ X-ray maps with profiles of high-precision point analyses.

A quantitative method requires a correction called ‘analytical standardization’ that transforms the number of collected photons (i.e., X-ray intensity) using either a semi-empirical Bence and Albee (1968) matrix correction (Clarke et al. 2001) or high-resolution spot analyses as internal standard (De Andrade et al. 2006). The technique of internal standardization provides accurate compositional maps and has recently been integrated into the software XMapTools (Lanari et al. 2014c). Quantitative compositional mapping allows measuring the natural variability of the mineral phases at the scale of a thin section and thus is useful in petrogenetic analysis (e.g., Kohn and Spear 2000). Compositional mapping has been successfully combined with multi-equilibrium thermobarometry (Vidal et al. 2006; Yamato et al. 2007; Fiannacca et al. 2012; Lanari et al. 2012, 2013, 2014a,b; Pourteau et al. 2013; Grosch et al. 2014; Loury et al. 2015, 2016; Trincal et al. 2015; Scheffer et al. 2016) and forward thermodynamic modeling (Abu-Alam et al. 2014; Lanari et al. 2017) or may be used to extract mineral modes (Cossio et al. 2002; Martin et al. 2013) and local compositions (Centrella et al. 2015; Riel and Lanari 2015; Mészáros et al. 2016).

Strategy to derive local bulk composition from X-ray maps using XMAPTOOLS

Local bulk composition can be easily estimated based on quantitative maps, for which the composition at each pixel is expressed in oxide wt%. The analytical procedure is detailed in Appendix 1. The local bulk composition of any desired part of the section mapped is spatially integrated, using the (oxide wt%) map and applying a density correction for each mineral phase identified. Density values are estimated using Theriak. This procedure is coded as a function available in XMapTools 2.3.1 and allows extracting the composition (in oxide wt%) of any domain directly from the compositional maps by polygonal boundaries selected by the user.

To illustrate the simplicity of this procedure, we selected an orthogneiss from the Glacier–Rafraý klippe in the Western Italian Alps (Burn 2016). X-ray maps were acquired using a beam current of 100 nA and dwell time of 70 ms. These maps were standardized using XMapTools 2.3.1 and the method described in Lanari et al. (2014c). The map size is 10.24×10.24 mm (corresponding to 1024×1024 pixels with a pixel size of $10 \mu\text{m}$; the total measurement time is ~ 42 h). This orthogneiss contains 38 vol% quartz, 33% albite, 21% phengite, 4% K-feldspar, 2% epidote, and 2% actinolite. The local bulk composition LBC1 was extracted from a square domain of $\sim 100 \text{mm}^2$ (dashed line in Fig. 11). To estimate the uncertainty in the composition resulting from the domain selection, a sensitivity test was performed using a Monte-Carlo simulation that randomly changed the position of the corners and thus the shape of the selected domain (Fig. 11). In this example 100 permutations were used with a displacement of each corner of ± 10 pixels (1σ assuming a Gaussian distribution). The composition of LBC1 is shown in Table 2 with the associated standard deviations and its relative uncertainty. The sensitivity test shows that there is very little variation ($<1\%$ for all the elements) in the composition due to this local domain selection.

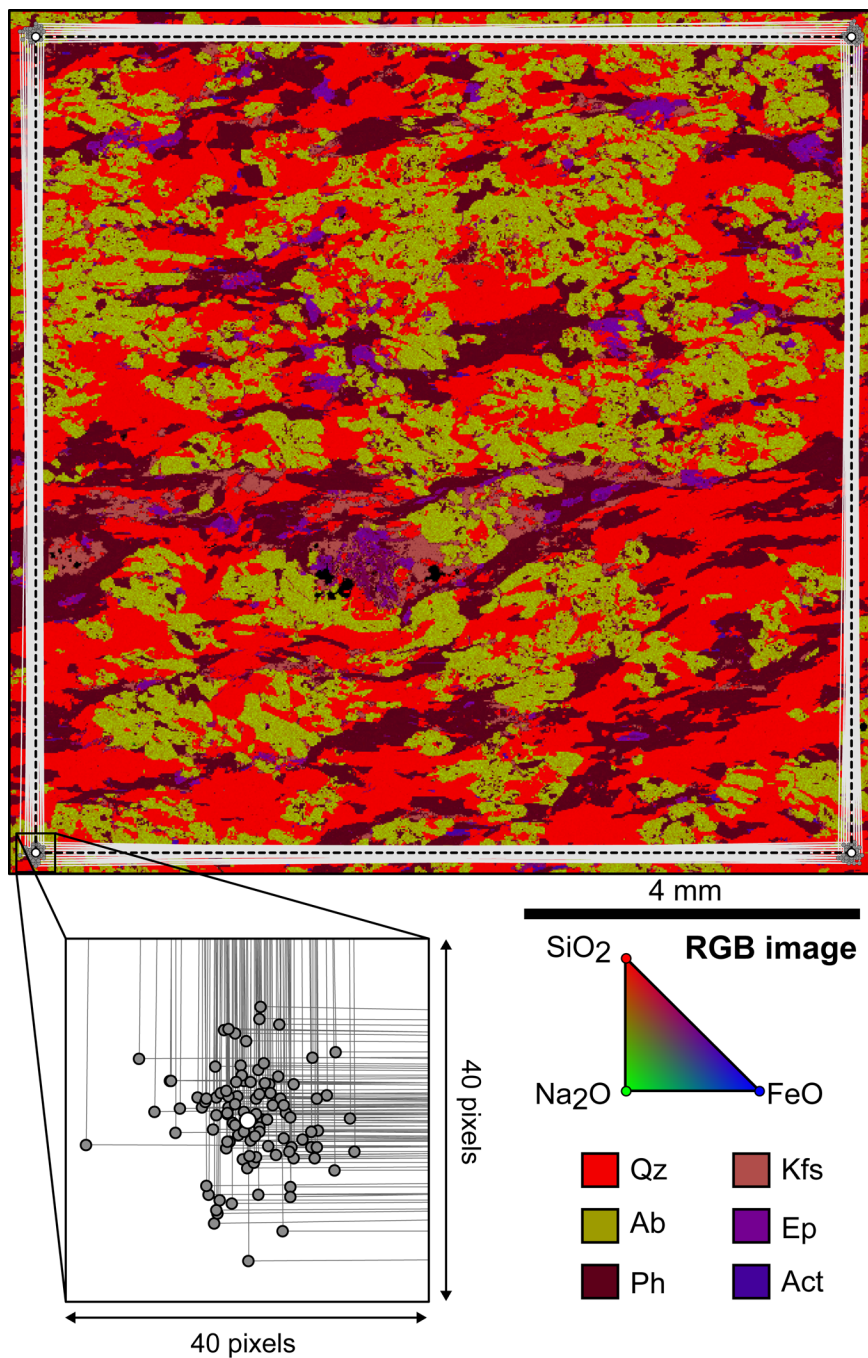


Figure 11. Estimation of local bulk composition for an orthogneiss from the Western Alps. Variably sized areas were considered, one delimitation shown by dashed black outline, gray lines in inset show variations used in sensitivity test performed by Monte-Carlo simulation (see text). Analysis based on XMapTools; the composite compositional map shown is color-coded in an RGB image displaying variations in SiO_2 - Na_2O - FeO , but any combination of oxides or element ratios could be chosen.

Table 2. Local bulk composition LBC1 of an orthogneiss from the Glacier-Rafraay Klippe in the Western Alps (see text) calculated using XMapTools (see Fig. 11). Abbreviations: Stdev. Standard deviation; Unc. Relative uncertainty.

	Mean	Stdev. (2 σ)	Unc. (%)
SiO ₂	75.420	0.057	0.076
Al ₂ O ₃	13.230	0.033	0.249
FeO	1.230	0.006	0.488
MgO	0.940	0.004	0.426
CaO	0.810	0.008	0.942
Na ₂ O	3.360	0.018	0.522
K ₂ O	3.090	0.017	0.551
Total	98.08		

Gibbs free energy minimization for the local bulk composition

A similar approach is used to propagate this relative uncertainty through the forward thermodynamic models. Computations were made using program Bingo-Antidote designed to estimate the optimal P - T conditions using equilibrium models (Lanari and Duesterhoeft 2016). The thermodynamic database JUN92.bs (Berman 1988 and subsequent updates) was selected for this test in the system SiO₂-Al₂O₃-FeO-Fe₂O₃-MgO-CaO-Na₂O-K₂O-H₂O. Excess oxygen (0.09 mol%) in the bulk composition was added to stabilize the observed amount of epidote. Negligible amounts of hematite (0.3 vol%) are predicted by the model (and ignored in the following). Mineral modes and compositions extracted from the domain LBC1 (Fig. 11) were modeled at 475 °C and 12.6 kbar (Fig. 12a), the estimated conditions of equilibration of the assemblage quartz + albite + phengite + K-feldspar + epidote. The dispersion ($\pm 2\sigma$) of the mineral modes predicted by the equilibrium model was estimated from 2000 permutations and is less than 1.6% (relative) for quartz, albite, phengite, and epidote, and 2.4% for K-feldspar (Fig. 12b). The corresponding information can also be extracted for mineral compositions. For example the model phengite composition is Si⁴⁺ = 3.481 \pm 0.002 atoms per formula unit (2 σ) and XMg = 0.874 \pm 0.008. This technique allows propagating the relative uncertainty in composition through the equilibrium models. As mentioned previously, few such sensitivity analyses have been reported (Kelsey and Hand 2015), and thus modeled modes have rarely been compared to observed mineral phases that contribute to the bulk composition (Warren and Waters 2006).

In the present example, an arbitrary $\sim 10 \times 10$ mm² domain was mapped and used to estimate the local bulk composition that was then taken as a reactive bulk composition for modeling. The overall quality of the model was excellent, which would seem to support the choice of this domain as an equilibrium domain. But is such a comparison sufficient to conclude that equilibrium was established at this spatial scale for the major elements? The answer is probably yes—at least for the elements of interest. However, for petrochronological studies the scale of equilibration for trace elements would be particularly relevant to verify whether slowly diffusing species attained uniform concentrations via an intergranular medium. To pursue this topic, the approach should be extended to use LA-ICP-MS quantitative maps. In this case a FCM would be needed as the accessory phases almost certainly act like porphyroblasts and trace constituents would not be part of the equilibration volume or reactive bulk composition.

Advantages of the micro-mapping approach

The approach described above can be used to test several textural domains from the same map dataset. Using Bingo-Antidote, it is thus possible to select a polygon and directly calculate the corresponding model assemblage, modes, and compositions for any P - T conditions.

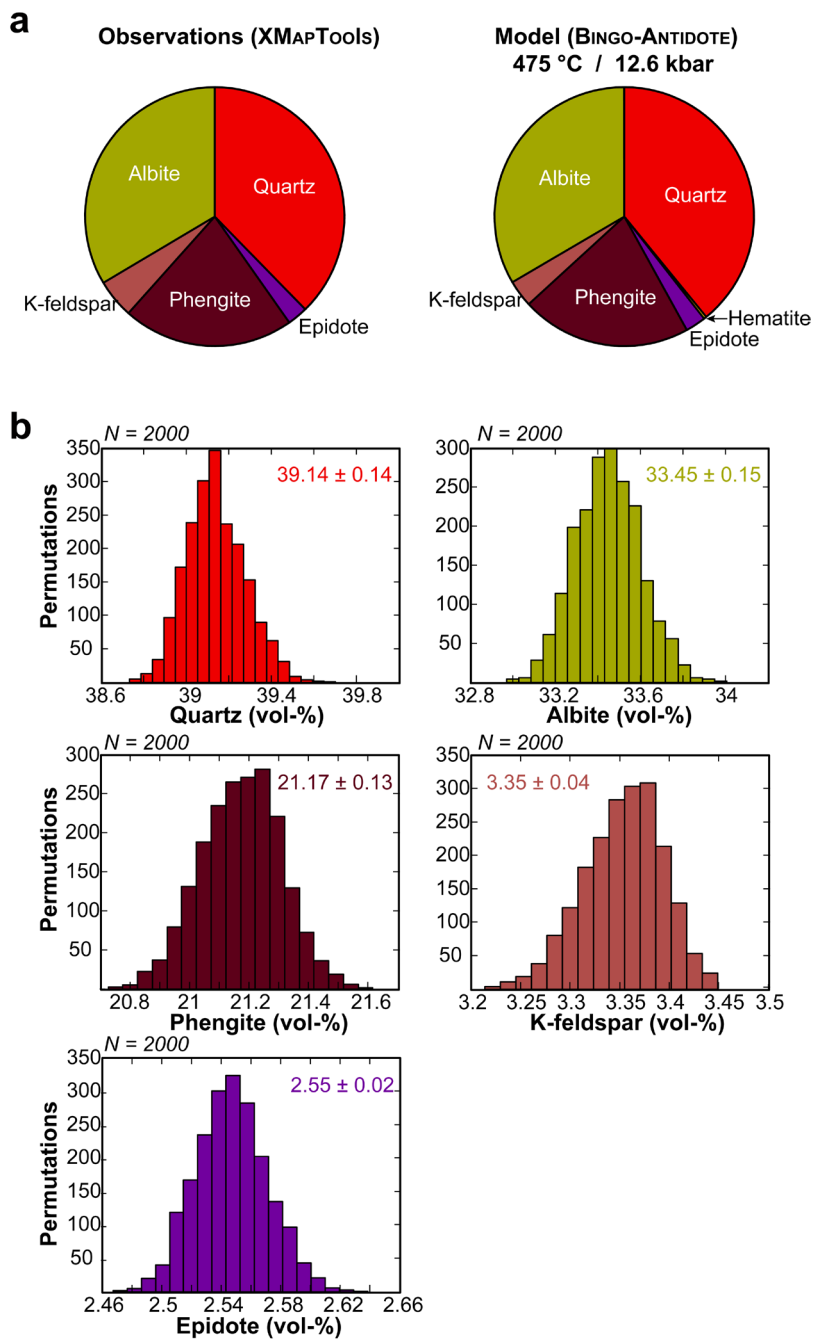


Figure 12. Gibbs free energy minimization using local bulk compositions (based on Fig. 11) and the program Bingo-Antidote. (a) Comparison between observed (left) and modeled (right) mineral modes. (b) Results of a sensitivity test (2000 permutations) performed to evaluate the effect of the domain selection on predicted mineral modes. Relative uncertainty in mode reported at 2σ level.

This strategy provides appropriate remedies to refine the estimation of the composition of the reactive part of a rock. For instance, most accessory phases are generally ignored in equilibrium phase diagrams, and this can lead to an erroneous bulk rock composition. Apatite is a good example because it contains >50 wt% CaO, and if a simplified system does not incorporate phosphorous, the amount of CaO from the bulk rock composition available for the other phases should be corrected for the CaO stored in apatite. However, correcting CaO based on P₂O₅ contents would introduce error if much monazite is present in the sample. This problem is easily solved using the micro-mapping approach: Apatite pixels can simply be ignored (a software option), and thus the CaO value of the local bulk composition is directly suitable for modeling. A similar approach can be used if any mineral present is considered non-reactive.

Potential artifacts affecting the local bulk composition estimates

To illustrate potential effects of some artifacts on the local bulk composition estimate and the equilibrium models, we use compositional maps of a mafic eclogite boudin from the Atbashi Range in the Kyrgyz South Tien Shan (Loury et al. 2015). The sample contains garnet porphyroblasts (with quartz and omphacite inclusions) in a matrix of omphacite, rutile, and ilmenite.

Geometric effects. Geometric effects arise as a consequence of sectioning a 3D texture and are most consequential if the surface fractions of successive growth zones of crystals cannot be linearly correlated with their volume fractions. For example, garnet typically has a dodecahedral crystal habit that can be approximated by a spherical geometry (Fig. 13b). If such a garnet grain is cut near its crystal center (see for example Fig. 1), any bulk crystal composition extracted from 2D compositional maps will overestimate the contribution of the core at the expense of the rim. If the cut is not equatorial, the section visible may not be representative of the zoning at all. The effect of such geometric bias is explored by comparing the composition of a single garnet grain extracted by first averaging from the 2D-map (Fig. 13a) or by converting the composition of each 2D-annulus to a 3D-hollow sphere (Fig. 13b) and then integrating these. This effect is generally neglected for local bulk composition estimates (Marmo et al. 2002) but for spherical domains it is judicious to use a 3D extrapolation (Mészáros et al. 2016). In the case of garnet from the mafic eclogite of the Atbashi Range, MnO is enriched in garnet core, and the average MnO composition of garnet is overestimated by 36% if integration is based on the 2D surface of a single grain (Fig. 13a). Similar deviations are observed for other elements (MgO -29%; and FeO +7%). For a map containing many grains, such geometric effects are partially compensated by stochastic sampling of different sections (Fig. 13c). In our example, integrating all of the garnet composition in 2D cuts the discrepancy in half, but it remains +16% in MnO, -17% in MgO, and +4% in FeO. It is also possible to evaluate the average garnet composition using a single crystal that is cut near the center (to be established with a diagnostic element such as Mn) and the spherical correction. Then this average garnet composition can be mixed with a complementary fraction of matrix for which an average composition is extracted from the maps.

Chemical equilibrium and the arbitrary choice of domains. Choosing or delimiting an appropriate local domain is obviously problem-dependent and usually non-trivial. For equilibrium thermodynamics to be applicable, the spatial domain selected for modelling should be no larger than the equilibration volume. (Of course any smaller domain might be selected). The problem is that the size limit is not known. Modellers often just hope that the domains are uniform in composition, i.e., that the mobility of the (slowest) components considered in their model was sufficient to equilibrate compositions over the chosen domain size. Generally, decisions should be based on (1) textural criteria such as the apparent homogeneity and representativeness of the domain compared to the entire specimen, or (2) independent transport criteria such as the maximum length scale of chemical equilibration predicted by the diffusion rate of Al (see Fig. 10).

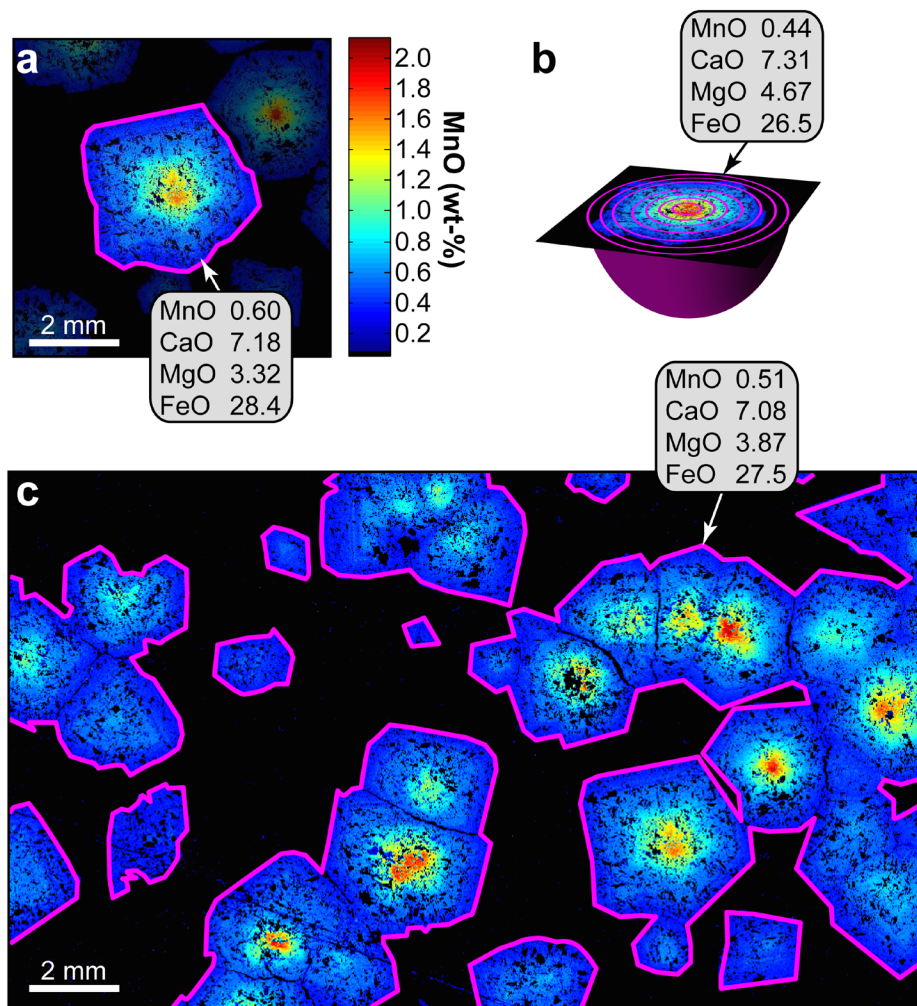


Figure 13. Average composition of garnet single grain estimated using XMapTools. (a) Method 1: 2D averaging of all the garnet pixels of a single crystal. (b) Method 2: 3D extrapolation using seven ellipsoids (details of procedure available in user guide of program, <http://www.xmaptools.com>). The 2D technique overestimates MnO (absolute: 0.16 wt%; relative difference (Δ) = 36%) and FeO (1.9 wt%; Δ 7%), underestimation of CaO (0.13 wt%; Δ 2%) and MgO (1.35 wt%; Δ 29%). (c) Method 3: 2D averaging of garnet pixels in all grains results in overestimation of MnO (0.07 wt%; Δ 16%) and FeO (1.0 wt%; Δ 4%) and underestimation of CaO (0.23 wt%; Δ 3%) and MgO (0.8 wt%; Δ 17%).

For a Kyrgyz mafic eclogite from Loury et al. (2015), the predicted length scale of intergranular diffusion of Al in 1 Ma, assuming a hydrous fluid present, is about 2 mm (Fig. 10). As garnet in this case crystallized at the expense of chlorite and lawsonite, it is likely that the intergranular medium was saturated in hydrous fluid, though perhaps only episodically, not for the entire 1 Ma. It is interesting to note that this spatial scale corresponds to the minimum distance between the centers of neighboring porphyroblasts observed in the section (Fig. 14). However the grains show remarkably regular chemical zoning in Ca and X_{Mg} ($Mg^{2+}/(Mg^{2+}+Fe^{2+})$) at the thin section scale (Fig. 14), suggesting that chemical equilibrium was maintained at the periphery of growing phases at all times (equilibrium control growth model assuming grain boundary equilibrium), which implies a much larger scale for chemical equilibration of the other major elements.

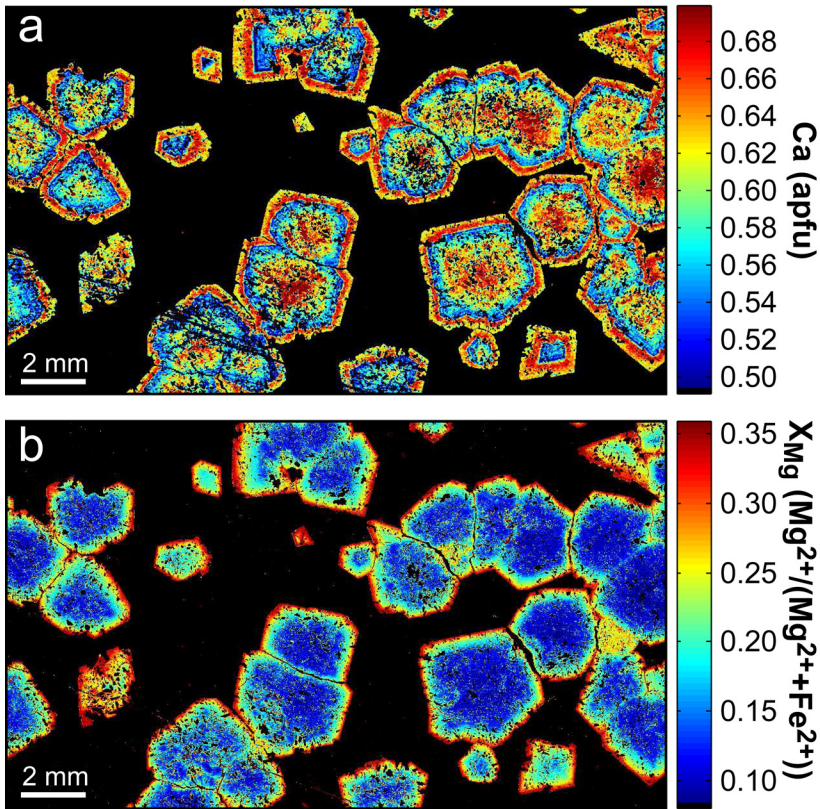


Figure 14. Compositional maps of garnet grains of a mafic eclogite boudin from the Atbashi Range in Kyrgyz South Tien Shan (Loury et al. 2015). Color code is for structural formula (apfu: atoms per formula unit); (a) Ca and (b) X_{Mg} .

Another strategy to ensure that the local bulk composition estimate is robust is to check the sensitivity of the composition and model predictions on the polygon selection (Fig. 15). The compositional map of the Kyrgyz mafic eclogite was sampled using a floating rectangular window, the size of which was increased from $6.8 \times 6.8 \text{ mm}^2$ to $20.5 \times 12 \text{ mm}^2$. The local bulk composition was successively calculated after each increment, and results are shown in Figure 15b. This experiment shows that the local bulk composition can be very sensitive to the area selected. The fluctuations are visible in the variable proportion of garnet (from 32 to 45 vol%, Fig. 15). Once some 80% of the area is integrated, the composition no longer changes significantly (<5% for all elements), as shown in the sensitivity tests.

Seeing such variations in the local bulk compositions (Fig. 15b), the critical question is: how sensitive are model predictions and P - T estimates? To appreciate the effect of this, the compositions of the four steps used in the above test (i.e., 18%, 50%, 80% and 100% of the area, Fig. 15) were used at 550°C and 25 kbar, with Bingo-Antidote and the thermodynamic dataset tc55.txt (Holland and Powell 1998) in the system SiO_2 - TiO_2 - Al_2O_3 - FeO - Fe_2O_3 - MnO - MgO - CaO - Na_2O ; the oxygen fugacity was controlled by the QFM buffer. The modeled mineral modes are in line with the mineral modes observed in the four areas (Fig. 15c), indicating that the predicted modes are correct. By contrast, the modeled garnet compositions are slightly different for the four models, with deviations of 0.03 in almandine

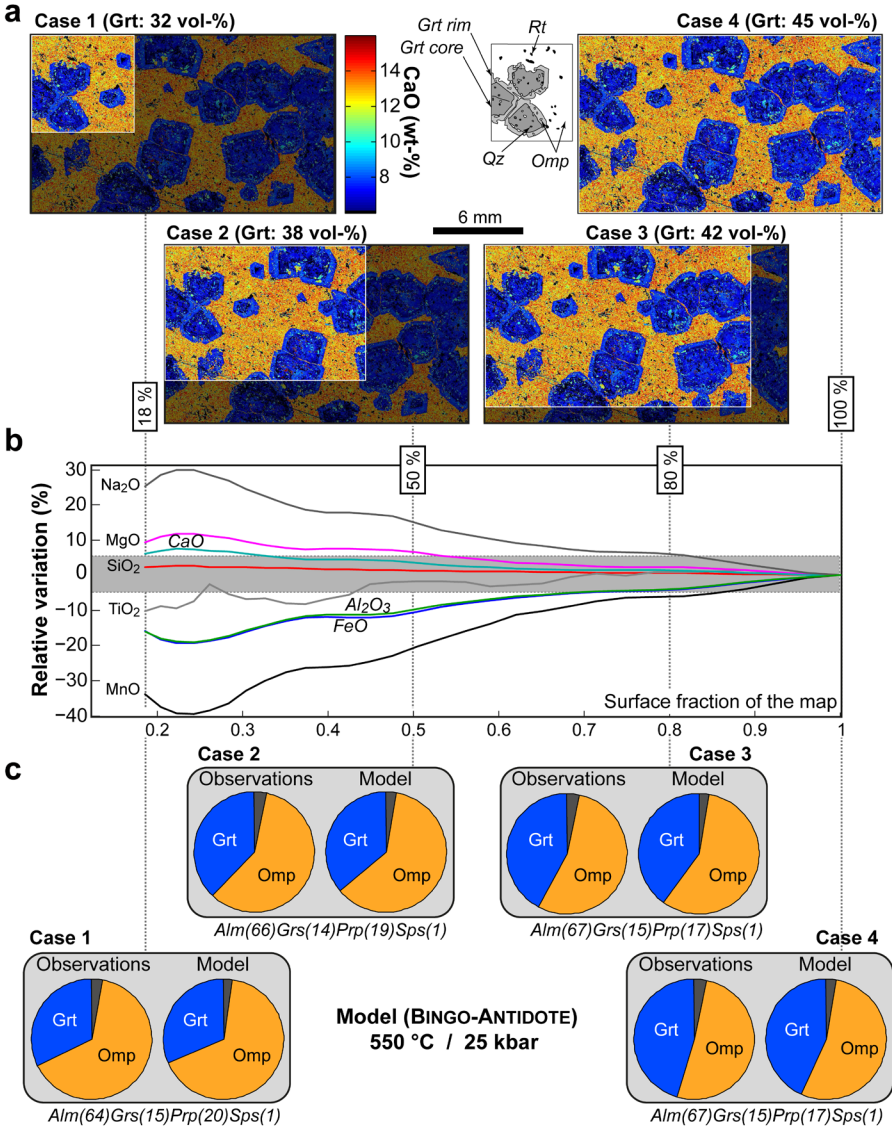


Figure 15. Estimated local bulk composition of a mafic eclogite boudin from the Atbashi Range in the Kyrgyz South Tien Shan (Loury et al. 2015). (a,b) The sensitivity test is based on different areas of a thin section (from 18% to 100% of the map surface). Note variation in predicted garnet mode. Compositional map shown for CaO (wt%); small inset: Grt: garnet, Omp: omphacite, Qz: quartz, Rt: rutile. (c) Modeled and observed mineral modes for the four cases shown in (a): 18%, 50%, 80% and 100% modeled at 550 °C and 25 kbar (see text).

and pyrope contents (Fig. 15c). To explore the bias of such differences to P - T estimates, the best isopleth intersection of a reference garnet core composition (Grt_{ref} corresponding to garnet predicted stable for the entire map composition; $\text{Alm}_{67}\text{Grs}_{15}\text{Prp}_{17}\text{Sps}_1$; case 4 in Fig. 15) was calculated for successive local bulk rock compositions using GrtMod (Fig. 16). Note that this example is used essentially to illustrate the concept: only one composition corresponding to a hypothetical garnet core is modeled, without expanding the case to FCM.

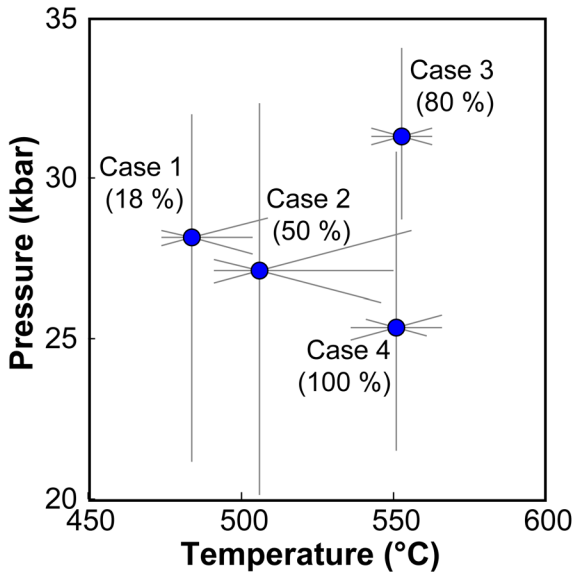


Figure 16. P - T conditions of Gr_{ref} (see text) for the four bulk compositions extracted from the areas shown in Figure 14 (Cases 1, 2, 3 and 4) computed with GrtMod. The errors bars show the relative uncertainty of the equilibrium model (i.e., isopleth position) resulting from typical uncertainties in garnet composition.

Gr_{ref} is predicted stable at lower temperature using the local composition of a small area ($480 \pm 25^\circ\text{C}$) compared to larger areas ($550 \pm 18^\circ\text{C}$). The errors bars reported in Figure 14 indicate the relative uncertainty of the equilibrium model (i.e., the isopleth position) resulting from typical uncertainties in garnet composition. The results presented here show that the differences in local bulk composition, depending on the domain size integrated, definitely can affect the garnet isopleths and hence P - T estimates. While somewhat technical and problem-dependent, this selection has significant consequences on P - T estimation.

The illustration example of the Kyrgyz mafic eclogite was selected because it contains several limits that have been intensively discussed in this review. First, it involves garnet porphyroblasts that are compositionally zoned, and an optimized strategy would require a FCM to obtain the P - T segment along which garnet grew. Second, the shape of garnet porphyroblasts requires the use of 3D extrapolation to avoid geometric effects on the local bulk composition estimates.

If a domain is assumed to be in chemical equilibrium at given P - T conditions, any smaller subdomain should yield a similar P - T estimate. Figure 16 shows substantial P - T differences for the domains shown in Figure 15, because garnet compositional zoning (disequilibrium) has a strong effect on the local bulk compositions. Apart from this, it is important to note that differences among thermodynamic data sets (standard state properties and solution models; not tested here) may also affect the P - T predictions.

Toward systematic quantitative trace element micro-mapping to address petrochronological problems

Quantitative mapping of diagnostic trace elements is crucial for many petrochronological applications. Over the past two decades, EMPA has been quite effectively used to produce such maps (e.g., Spear and Kohn 1996; Chernoff and Carlson 1999), but recent improvements in LA-ICP-MS analysis and software support (Paul et al. 2012; Rittner and Müller 2012) have fostered applications using quantitative maps of trace elements and isotopes (Becker et al. 2007; Woodhead et al. 2007; Stowell et al. 2010; Duval et al. 2011; Netting et al. 2011; Šelih and van Elteren 2011; Peng et al. 2012; Paul et al. 2014; Gatewood et al. 2015; Ubide et al. 2015).

For instance a garnet from the Peaked Hill shear zone, Reynolds Range, central Australia, has been mapped by this technique (Raimondo et al. 2017), with successive raster images of the focused laser beam stitched together to form a 2D representation of the trace element distribution. Quantification was initially performed using Iolite (Woodhead et al. 2007; Paton et al. 2011), and subsequent image processing and manipulation by XMapTools (Lanari et al. 2014c). The maps reveal significant decoupling between the major and trace element zoning patterns, with smooth radial zoning in Fe, Mg, Ca and Mn juxtaposed against a discrete annular structure and successive satellite peaks for REEs and Cr (Fig. 17). Importantly, the growth and dissolution of accessory phases can be directly linked to garnet evolution through the superposition of sharp satellite peaks in Zr and HREE (zircon) and P, Th and LREEs (monazite). Such micron-scale features are clearly resolved by trace element mapping, but easy to miss with more coarsely spaced spot analyses. Thus the increased spatial resolution and mass range of LA-ICP-MS mapping offer a powerful means to place garnet growth in a specific paragenetic context and integrate it with temporal constraints provided by accessory phase geochronometers or direct Lu–Hf/Sm–Nd dating.

CONCLUSIONS AND PERSPECTIVES

The examples presented in this review indicate that care is needed when modeling a rock with evident compositional heterogeneity or textural domains. Textural evidence in rocks— notably mineral zoning—shows that rocks adapt to changes in conditions during their evolution, but that equilibration is limited by kinetics of transport. Nonetheless, equilibrium models—and especially thermodynamic forward models—remain powerful for petrogenetic analysis and allow the retrieval of P – T conditions, provided that partial and local assemblages are analyzed.

Zoned porphyroblasts can significantly fractionate the reactive bulk composition, and this effect must be included in setting up FCM's. In the case of garnet, it has been shown that ECM's significantly overestimate the predicted modes and affect the P – T estimates made by isopleths thermobarometry. Dating porphyroblast growth remains attractive, based on textural correlation and in situ dating techniques. Correlation efforts to link ages with porphyroblast growth (or resorption) conditions can profit from quantitative element mapping of both major and trace elements. Documenting how concentrations in REE, Y, Th, and U evolve in successive growth zones of the host and in the included accessories should be useful for testing whether or not host and inclusions are in exchange equilibrium (i.e., may or may not be regarded as coeval). More fundamentally, such combined analysis promises much needed insight into the mobility of trace elements relative to major elements.

A bulk rock composition determined by XRF analysis of an entire sample can be very far from the composition of a local assemblage, hence thermobarometry based on isopleths will be flawed, even observed phase relations may compare poorly with predictions. Instead, the reactive bulk composition must be approximated by taking account the textural evidence and preserved local mineral compositions. X-ray maps yield a solid basis to estimate the local bulk composition, if the spatial domain to be modeled is carefully delimited in thin section. Predictions from local equilibrium models must be critically evaluated, checking the textural and mineralogical record preserved in a sample against the computed phase relations for it. Using a program such as Bingo-Antidote also allows the sensitivity of predictions to the chosen domain boundaries to be tested. In our experience the local composition needs to be iteratively refined, or it may turn out that different chemical subsystems should be chosen to analyze different parts of a rock's evolution. The goal must be to gain a fairly detailed understanding of the petrogenetic stages visible in a sample, which ensures that P – T conditions estimated using isopleths are robust. Such a basis allows a meaningful strategy to select datable (sub)grains for in situ analysis, which we consider critical to trustworthy petrochronology.

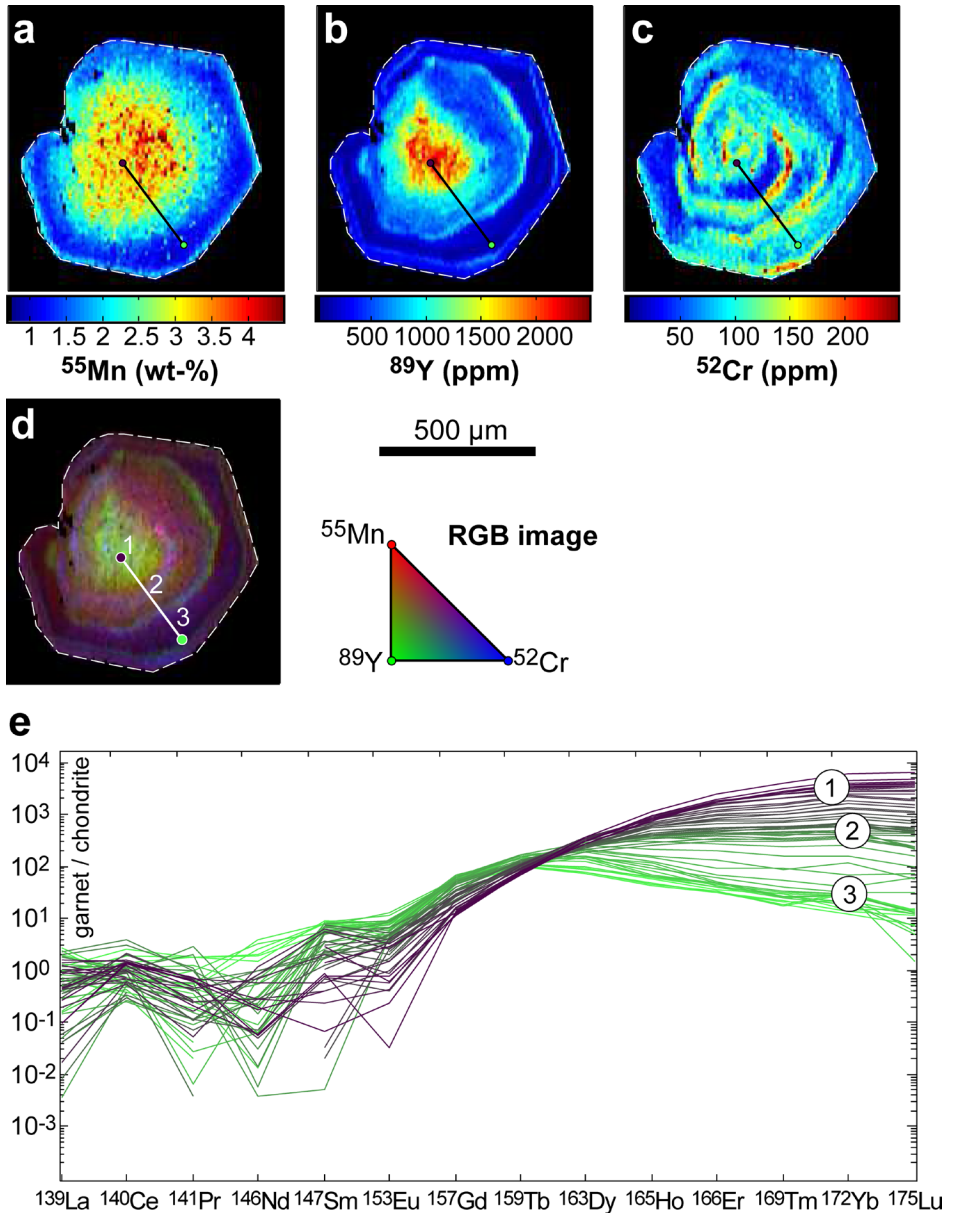


Figure 17. Minor and trace element compositional maps of a garnet grain from the Peaked Hill shear zone, Reynolds Range (Raimondo et al. 2017), central Australia. (a) Mn in wt%; (b) Y in ppm; (c) Cr in ppm; (d) Composite RGB image; (e) Chondrite-normalized REE patterns of garnet along the profile drawn in a, b, c and d (one curve in (e) per pixel). Concentrations given are for the element of interest, isotope numbers show which isotope was used to monitor element abundance.

Some elements are far less mobile than others, and gradients in concentration (and thus in chemical potential) may be preserved that render equilibrium modeling inappropriate, i.e., relatively immobile species (including some trace elements) may have to be excluded.

At present, there is limited knowledge regarding the mobility of many trace elements, notably for actinides, Pb and REE that are critical to chronology. It remains a challenge to develop approaches that integrate local equilibrium models for domains in which these elements show evidence of limited transport. To improve our understanding, concentration gradients, both within and among domains, should be documented for elements with very different transport properties (ionic charge and size of species dominant for transport). Such maps provide integrals over the relative mobility and may allow us to distinguish chemical subsystems for which local equilibrium modeling is reliable vs. those that are sensitive to kinetics. To reconstruct local chemical potential gradients, it would be intriguing to invert the model, i.e., the compositional gradient that can be observed between two textural domains. Extending earlier studies (Carlson 2002), the characterization of the frozen-in gradients will help quantify extents of disequilibrium.

ACKNOWLEDGMENTS

We thank M. Burn, F. Giuntoli, F. Guillot, C. Loury and T. Raimondo for providing sample information and compositional maps used in Figures 2 (MB, FGi, FGU), 11 (MB), 13–14–15 (CL), 17 (TR). We acknowledge stimulating discussions with R. Berman, C. de Capitani, E. Dueterhoeft, J. Hermann and D. Rubatto. Reviews from H. Stowell and G. Clarke, as well as helpful comments from M. Kohn that led us to improve this paper are gratefully acknowledged, as is Matt's editorial handling. The Swiss National Science Foundation (Project 200020-146175) and the Faculty of Science of the University of Bern have supported work presented here.

APPENDIX 1—LOCAL BULK COMPOSITIONS FROM OXIDE WEIGHT PERCENTAGE MAPS

Let us consider a domain of rock composed of three mineral phases Min_1 , Min_2 and Min_3 , each homogeneous in composition C_1^i , C_2^i and C_3^i of the oxides of the element i . C is expressed in oxide wt%. This is convenient here because chemical analyses of silicate minerals are commonly reported in wt% of the oxides determined. The local bulk composition of this domain C_{LB} can be calculated as:

$$C_{LB} = w_1 C_1^i + w_2 C_2^i + w_3 C_3^i \quad (A1)$$

With w_1 , w_2 and w_3 the mass fractions of the mineral phases Min_1 , Min_2 and Min_3 . This relation can be generalized for a map of a given domain containing n pixels:

$$C_{LB} = \sum_{j=1}^n w_j C_j^i \quad (A2)$$

w_j and C_j^i are the mass fraction and composition in oxide weight percentage of pixel j . The use of Relation (A2) is not straightforward, as it requires the knowledge of the mass fraction of every pixel that may belong to different phases, each with a different molar mass.

On the other hand, the pixel fraction of a phase k is a good approximation of the surface covered by this phase and can be extrapolated to a volume fraction. To a first approximation, it is often assumed that:

$$v_k = s_k \quad (A3)$$

In metamorphic petrology, this relation may be reasonable if (i) the sample was sectioned perpendicular to the foliation or schistosity, (ii) the compositional map is acquired on an

unaltered rock surface devoid of local compositional heterogeneities, (iii) the size of the map is sufficient to ensure good sampling, (iv) the resolution of the map is high enough to avoid issues with the smaller grain size population, and (v) 3D effects are negligible. Possible pitfalls and issues are discussed under 'Potential artifacts affecting the local bulk composition estimates'. The relationship between the mass fraction and the volume fraction is:

$$w_k = \frac{\rho_k}{\rho_{\text{mixture}}} v_k \quad (\text{A4})$$

with ρ_k being the density of the phase k and the average density ρ_{mixture} of the domain. Integrating the density correction in Equation (A2) leads to a more convenient expression of the local bulk composition of the domain:

$$C_{\text{LB}} = \sum_{j=1}^n \frac{\rho_k}{\rho_{\text{mixture}}} v_j C_j^i \quad (\text{A5})$$

From this relationship it is possible to extract the local bulk composition of a domain using the average density of every phase involved.

In case of multi-phase assemblages the density correction is required to predict accurate local bulk compositions. For example, most of the studies discussed in this review did not correct for density differences between the considered minerals (M. Tóth et al. 2000; Marmo et al. 2002; Brouwer and Engi 2005; Cenki-Tok et al. 2016), and this can lead to large discrepancies for elements sequestered by dense mineral phases (e.g., Fe in magnetite or garnet).

Bulk rock compositions can also be extracted from oxide weight percentage maps. In this case, a domain with as many grains as practical should be selected. Based on the two examples discussed in this paper, we suggest that the width of the selected surface must be at least 8–10 times the 'average' size of the largest grains. This criterion (i.e., >65 times the 'average' grain surface) ensures that the composition is fairly representative of the entire composition of the domain, as long as the section is uniform in mineral assemblage.

REFERENCES

- Abu-Alam TS, Hassan M, Stüwe K, Meyer SE, Passchier CW (2014) Multistage tectonism and metamorphism during Gondwana collision: Baladiyah Complex, Saudi Arabia. *J Petrol* 55:1941–1964, doi:10.1093/ptrology/egu046
- Ague JJ, Axler JA (2016) Interface coupled dissolution–precipitation in garnet from subducted granulites and ultrahigh-pressure rocks revealed by phosphorous, sodium, and titanium zonation. *Am Mineral* 101:1696–1699, doi:10.2138/am-2016-5707
- Anderson DE, Olimpio JC (1977) Progressive homogenization of metamorphic garnets, South Morar, Scotland; evidence for volume diffusion. *Can Mineral* 15:205–216
- Atherton MP (1968) The variation in garnet, biotite and chlorite composition in medium grade pelitic rocks from the Dalradian, Scotland, with particular reference to the zonation in garnet. *Contrib Mineral Petrol* 18:347–371, doi:10.1007/bf00399696
- Ballevre M, Pitra P, Bohn M (2003) Lawsonite growth in the epidote blueschists from the Ile de Groix (Armorican Massif, France): a potential geobarometer. *J Metamorph Geol* 21:723–735, doi:10.1046/j.1525-1314.2003.00474.x
- Baxter EF, Caddick MJ, Dragovic B (2017) Garnet: A rock-forming mineral petrochronometer. *Rev Mineral Geochem* 83:469–533
- Becker JS, Zoriy M, Becker JS, Dobrowolska J, Matusch A (2007) Laser ablation inductively coupled plasma mass spectrometry (LA-ICP-MS) in elemental imaging of biological tissues and in proteomics. *J Anal At Spectrom* 22:736–744, doi:10.1039/B701558E
- Beinlich A, Klemd R, John T, Gao J (2010) Trace-element mobilization during Ca-metasomatism along a major fluid conduit: Eclogitization of blueschist as a consequence of fluid–rock interaction. *Geochim Cosmochim Acta* 74:1892–1922, doi:10.1016/j.gca.2009.12.011

- Bell TH, Rubenach MJ, Fleming PD (1986) Porphyroblast nucleation, growth and dissolution in regional metamorphic rocks as a function of deformation partitioning during foliation development. *J Metamorph Geol* 4:37–67, doi:10.1111/j.1525–1314.1986.tb00337.x
- Bence AE, Albee AL (1968) Empirical correction factors for the electron microanalysis of silicates and oxides. *J Geol* 76:382–403
- Berman RG (1988) Internally consistent thermodynamic data for minerals in the system $\text{Na}_2\text{O}-\text{K}_2\text{O}-\text{CaO}-\text{MgO}-\text{FeO}-\text{Fe}_2\text{O}_3-\text{Al}_2\text{O}_3-\text{SiO}_2-\text{TiO}_2-\text{H}_2\text{O}-\text{CO}_2$. *J Petrol* 29:445–522
- Bowen NL (1913) The melting phenomena of the plagioclase feldspars. *Am J Sci Ser 4* 35:577–599, doi:10.2475/ajs.s4-35.210.577
- Brodie KH, Rutter EH (1985) On the relationship between deformation and metamorphism, with special reference to the behavior of basic rocks. *In: Metamorphic Reactions: Kinetics, Textures, and Deformation*. Thompson AB, Rubie DC (eds). Springer New York, p.138–179
- Brouwer FM, Engi M (2005) Staurolite and other high-alumina phases in Alpine eclogite: Analysis of domain evolution. *Can Mineral* 43:105–128
- Brovarone AV, Groppo C, Hetenyi G, Compagnoni R, Malavieille J (2011) Coexistence of lawsonite-bearing eclogite and blueschist: phase equilibria modelling of Alpine Corsica metabasalts and petrological evolution of subducting slabs. *J Metamorph Geol* 29:583–600, doi:10.1111/j.1525–1314.2011.00931.x
- Brown M (2002) Retrograde processes in migmatites and granulites revisited. *J Metam. Geol* 20:25–40
- Burn M (2016) LA-ICP-QMS Th–U/Pb allanite dating: methods and applications. PhD thesis University of Bern
- Caddick MJ, Kohn MJ (2013) Garnet: Witness to the evolution of destructive plate boundaries. *Elements* 9:427–432, doi:10.2113/gselements.9.6.427
- Caddick MJ, Bickle MJ, Harris NBW, Holland TJB, Horstwood MSA, Parrish RR, Ahmad T (2007) Burial and exhumation history of a Lesser Himalayan schist: Recording the formation of an inverted metamorphic sequence in NW India. *Earth Planet Sci Lett* 264:375–390
- Caddick MJ, Konopásek J, Thompson AB (2010) Preservation of garnet growth zoning and the duration of prograde metamorphism. *J Petrol* 51:2327–2347, doi:10.1093/petrology/egg059
- Carlson WD (1989) The significance of intergranular diffusion to the mechanisms and kinetics of porphyroblast crystallization. *Contrib Mineral Petrol* 103:1–24
- Carlson WD (2002) Scales of disequilibrium and rates of equilibration during metamorphism. *Am Mineral* 87:185–204, doi:10.2138/am-2002-2-301
- Carlson WD (2010) Dependence of reaction kinetics on H_2O activity as inferred from rates of intergranular diffusion of aluminium. *J Metamorph Geol* 28:735–752, doi:10.1111/j.1525–1314.2010.00886.x
- Carlson WD, Johnson CD (1991) Coronal reaction textures in garnet amphibolites of the Llano Uplift. *Am Mineral* 76:756–772
- Carlson WD, Pattison DRM, Caddick MJ (2015) Beyond the equilibrium paradigm: How consideration of kinetics enhances metamorphic interpretation. *Am Mineral* 100:1659–1667, doi:10.2138/am-2015-5097
- Carmichael DM (1969) On the mechanism of prograde metamorphic reactions in quartz-bearing pelitic rocks. *Contrib Mineral Petrol* 20:244–267
- Centki-Tok B, Berger A, Gueydan F (2016) Formation and preservation of biotite-rich microdomains in high-temperature rocks from the Antananarivo Block, Madagascar. *Int J Earth Sci* 105:1471–1483, doi:10.1007/s00531-015-1265-0
- Centrella S, Austrheim H, Putnis A (2015) Coupled mass transfer through a fluid phase and volume preservation during the hydration of granulite: An example from the Bergen Arcs, Norway. *Lithos* 236–237:245–255, doi:10.1016/j.lithos.2015.09.010
- Chapman AD, Luffi PI, Saleeby JB, Petersen S (2011) Metamorphic evolution, partial melting and rapid exhumation above an ancient flat slab: insights from the San Emigdio Schist, southern California. *J Metamorph Geol* 29:601–626, doi:10.1111/j.1525–1314.2011.00932.x
- Cheng H, Cao D (2015) Protracted garnet growth in high-P eclogite: constraints from multiple geochronology and P – T pseudosection. *J Metamorph Geol* 33:613–632, doi:10.1111/jmg.12136
- Cheng H, Nakamura E, Kobayashi K, Zhou Z (2007) Origin of atoll garnets in eclogites and implications for the redistribution of trace elements during slab exhumation in a continental subduction zone. *Am Mineral* 92:1119–1129, doi:10.2138/am.2007.2343
- Chernoff CB, Carlson WD (1999) Trace element zoning as a record of chemical disequilibrium during garnet growth. *Geology* 27:555–558
- Clarke GL, Daczko NR, Nockolds C (2001) A method for applying matrix corrections to X-ray intensity maps using the Bence–Albee algorithm and Matlab. *J Metamorph Geol* 19:635–644, doi:10.1046/j.0263–4929.2001.00336.x
- Connolly JAD (1990) Multivariate phase diagrams: An algorithm based on generalized thermodynamics. *Am J Sci* 290:666–718
- Connolly JAD (2005) Computation of phase equilibria by linear programming: a tool for geodynamic modeling and its application to subduction zone decarbonation. *Earth Planet Sci Lett* 236:524–541

- Cossio R, Borghi A, Ruffini R (2002) Quantitative modal determination of geological samples based on X-ray multielemental map acquisition. *Microsc Microanal* 8:139–149, doi:10.1017/S1431927601020062
- Cosslett VE, Duncumb P (1956) Micro-analysis by a flying-spot X-ray method. *Nature* 177:1172–1173
- Cygan RT, Lasaga AC (1982) Crystal growth and the formation of chemical zoning in garnets. *Contrib Mineral Petrol* 79:187–200, doi:10.1007/bf01132887
- Davis PB, Whitney DL (2006) Petrogenesis of lawsonite and epidote eclogite and blueschist, Sivrihisar Massif, Turkey. *J Metamorph Geol* 24:823–849
- de Andrade V, Vidal O, Lewin E, O'Brien P, Agard P (2006) Quantification of electron microprobe compositional maps of rock thin sections: an optimized method and examples. *J Metamorph Geol* 24:655–668, doi:10.1111/j.1525–1314.2006.00660.x
- de Béthune P, Laduron D, Bocquet J (1975) Diffusion processes in resorbed garnets. *Contrib Mineral Petrol* 50:197–204, doi:10.1007/bf00371039
- de Capitani C, Brown TH (1987) The computation of chemical equilibrium in complex systems containing non-ideal solutions. *Geochim Cosmochim Acta* 51:2639–2652
- de Capitani C, Petrakakis K (2010) The computation of equilibrium assemblage diagrams with Theriak/Domino software. *Am Mineral* 95:1006–1016, doi:10.2138/am.2010.3354
- DeVore GW (1955) The role of adsorption in the fractionation and distribution of elements. *J Geol* 63:159–190, doi:10.1086/626242
- Dragovic B, Samanta LM, Baxter EF, Selverstone J (2012) Using garnet to constrain the duration and rate of water-releasing metamorphic reactions during subduction: An example from Sifnos, Greece. *Chem Geol* 314–317:9–22, doi:10.1016/j.chemgeo.2012.04.016
- Dupuis M (2012) Macro- et microstructure de l'éventail briangonnais. MSc thesis Université de Lille 1
- Duval M, Aubert M, Hellstrom J, Grün R (2011) High resolution LA-ICP-MS mapping of U and Th isotopes in an early Pleistocene equid tooth from Fuente Nueva-3 (Orce, Andalusia, Spain). *Quat Geochronol* 6:458–467, doi:10.1016/j.quageo.2011.04.002
- Elvevold S, Gilotti JA (2000) Pressure–temperature evolution of retrogressed kyanite eclogites, Weinschenk Island, North–East Greenland Caledonides. *Lithos* 53:127–147, doi:10.1016/S0024-4937(00)00014–1
- Erambert M, Austrheim H (1993) The effect of fluid and deformation on zoning and inclusion patterns in poly-metamorphic garnets. *Contrib Mineral Petrol* 115:204–214, doi:10.1007/bf00321220
- Evans TP (2004) A method for calculating effective bulk composition modification due to crystal fractionation in garnet-bearing schist; implications for isopleth thermobarometry *J Metamorph Geol* 22:547–557
- Evans KA, Bickle MJ (2005) An investigation of the relationship between bulk composition, inferred reaction progress and fluid flow parameters for layered micaceous carbonates from Maine, U.S.A. *J Metamorph Geol* 23:181–197
- Faryad SW, Klápová H, Nosal L (2010) Mechanism of formation of atoll garnet during high-pressure metamorphism. *Mineral Mag* 74:111–126, doi:10.1180/minmag.2010.074.1.111
- Fiannacca P, Lo Pò D, Ortolano G, Cirrincione R, Pezzino A (2012) Thermodynamic modeling assisted by multivariate statistical image analysis as a tool for unraveling metamorphic *P–T–d* evolution: an example from ilmenite–garnet-bearing metapelite of the Peloritani Mountains, Southern Italy. *Mineral Petrol* 106:151–171, doi:10.1007/s00710-012-0228-4
- Fisher GW (1973) Nonequilibrium thermodynamics as a model for diffusion-controlled metamorphic processes. *Am J Sci* 273:897–924, doi:10.2475/ajs.273.10.897
- Fisher GW, Lasaga AC (1981) Irreversible thermodynamics in petrology. *Rev Mineral Geochem* 8:171–207
- Fitzsimons ICW, Kinny PD, Wetherley S, Hollingsworth DA (2005) Bulk chemical control on metamorphic monazite growth in pelitic schists and implications for U–Pb age data. *J Metamorph Geol* 23:261–277, doi:10.1111/j.1525–1314.2005.00575.x
- Fletcher RC (1977) Quantitative theory for metamorphic differentiation in development of crenulation cleavage. *Geology* 5:185–187, doi:10.1130/0091–7613
- Florence FP, Spear FS (1991) Effects of diffusional modification of garnet growth zoning on *PT* path calculations. *Contrib Mineral Petrol* 107:487–500
- Foster CT (1977) Mass transfer in sillimanite-bearing pelitic schists near Rangeley, Maine. *Am Mineral* 62:727–746
- Foster CT (1981) A thermodynamic model of mineral segregations in the lower sillimanite zone near Rangeley, Maine. *Am Mineral* 66:260–277
- Foster CT (1983) Thermodynamic models of biotite pseudomorphs after staurolite. *Am Mineral* 68:389–397
- Foster CT (1986) Thermodynamic models of reactions involving garnet in a sillimanite/staurolite schist. *Mineral Mag* 50:427–439
- Foster CT (1991) The role of biotite as a catalyst in reaction mechanisms that form sillimanite. *Can Mineral* 29:943–963
- Foster CT (1999) Forward modeling of metamorphic textures. *Can Mineral* 37:415–429
- Foster G, Kinny P, Vance D, Prince C, Harris N (2000) The significance of monazite U–Th–Pb age data in metamorphic assemblages; a combined study of monazite and garnet chronometry. *Earth Planet Sci Lett* 181:327–340

- Foster G, Parrish RR, Horstwood MSA, Chenery S, Pyle J, Gibson HD (2004) The generation of prograde P - T - t points and paths; a textural, compositional, and chronological study of metamorphic monazite. *Earth Planet Sci Lett* 228:125–142, doi:10.1016/j.epsl.2004.09.024
- Gaidies F, Abart R, de Capitani C, Schuster R, Connolly JAD, Reusser E (2006) Characterization of polymetamorphism in the Austroalpine basement east of the Tauern Window using garnet isopleth thermobarometry. *J Metamorph Geol* 24:451–475, doi:10.1111/j.1525–1314.2006.00648.x
- Gaidies F, de Capitani C, Abart R (2008) THERIA_G: a software program to numerically model prograde garnet growth. *Contrib Mineral Petrol* 155:657–671, doi:10.1007/s00410-007-0263-z
- Gaidies F, Pattison DRM, de Capitani C (2011) Toward a quantitative model of metamorphic nucleation and growth. *Contrib Mineral Petrol* 162:975–993, doi:10.1007/s00410-011-0635-2
- Ganguly J (2010) Cation diffusion kinetics in aluminosilicate garnets and geological applications. *Rev Mineral Geochem* 72:559–601
- Ganguly J, Chakraborty S, Sharp TG, Rumble D (1996) Constraint on the time scale of biotite-grade metamorphism during Acadian orogeny from a natural garnet–garnet diffusion couple. *Am Mineral* 81:1208–1216
- Gatewood MP, Dragovic B, Stowell HH, Baxter EF, Hirsch DM, Bloom R (2015) Evaluating chemical equilibrium in metamorphic rocks using major element and Sm–Nd isotopic age zoning in garnet, Townshend Dam, Vermont, USA. *Chemical Geology* 401:151–168, doi:10.1016/j.chemgeo.2015.02.017
- Giuntoli F (2016) Assembly of continental fragments during subduction at HP: Metamorphic history of the central Sesia Zone (NW Alps). PhD thesis University of Bern
- Goldschmidt VM (1911) Die Kontaktmetamorphose im Kristianiagebiet. In Kommission bei J. Dybwad, Kristiania
- Goncalves P, Oliot E, Marquer D, Connolly JAD (2012) Role of chemical processes on shear zone formation: an example from the Grimsel metagranodiorite (Aar Massif, Central Alps). *J Metamorph Geol* 30:703–722, doi:10.1111/j.1525–1314.2012.00991.x
- Gottschalk M (1996) Internally consistent thermodynamic data for rock-forming minerals in the system SiO_2 – TiO_2 – Al_2O_3 – Fe_2O_3 – CaO – MgO – FeO – K_2O – Na_2O – H_2O – CO_2 . *Eur J Mineral* 9:175–223, doi:10.1127/ejm/9/1/0175
- Grand'Homme A, Janots E, Seydoux-Guillaume A-M, Guillaume D, Bosse V, Magnin V (2016) Partial resetting of the U–Th–Pb systems in experimentally altered monazite: Nanoscale evidence of incomplete replacement. *Geology* 44:431–434
- Greenfield JE (1997) Migmatite formation at Mt Stafford, central Australia. PhD thesis, University of Sidney
- Greenfield JE, Clarke GL, Bland M, Clark DJ (1996) In-situ migmatite and hybrid diatexite at Mt Stafford, central Australia. *J Metamorph Geol* 14:413–426, doi:10.1046/j.1525–1314.1996.06002.x
- Greenwood HJ (1967) The N-dimensional tie-line problem. *Geochim Cosmochim Acta* 31:465–490
- Groppo C, Castelli D (2010) Prograde P - T evolution of a lawsonite eclogite from the Monviso meta-ophiolite (Western Alps): Dehydration and redox reactions during subduction of oceanic FeTi-oxide gabbro. *J Petrol* 51:2489–2514, doi:10.1093/petrology/egq065
- Groppo C, Lombardo B, Rolfo F, Pertusati P (2007) Clockwise exhumation path of granulitized eclogites from the Ama Drime range (Eastern Himalayas). *J Metamorph Geol* 25:51–75, doi:10.1111/j.1525–1314.2006.00678.x
- Grosch EG, McLoughlin N, Lanari P, Erambert M, Vidal O (2014) Microscale mapping of alteration conditions and potential biosignatures in basaltic–ultramafic rocks on early earth and beyond. *Astrobiology* 14:216–228, doi:10.1089/ast.2013.1116
- Guevara VE, Caddick MJ (2016) Shooting at a moving target: phase equilibria modelling of high-temperature metamorphism. *J Metamorph Geol* 34:209–235, doi:10.1111/jmg.12179
- Harrison TM, Catlos EJ, Montel J-M (2002) U–Th–Pb dating of phosphate minerals. *Rev Mineral Geochem* 48:524–558, doi:10.2138/rmg.2002.48.14
- Harvey J, Baxter EF (2009) An improved method for TIMS high precision neodymium isotope analysis of very small aliquots (1–10 ng). *Chem Geol* 258:251–257, doi:10.1016/j.chemgeo.2008.10.024
- Hickmott DD, Shimizu N, Spear FS, Selverstone J (1987) Trace-element zoning in a metamorphic garnet. *Geology* 15:573–576, doi:10.1130/0091–7613(1987)15<573:tziang>2.0.co;2
- Hoisch TD, Wells ML, Grove M (2008) Age trends in garnet-hosted monazite inclusions from upper amphibolite facies schist in the northern Grouse Creek Mountains, Utah. *Geochimica et Cosmochimica Acta* 72:5505–5520, doi:10.1016/j.gca.2008.08.012
- Holland TJB, Powell R (1988) An internally consistent thermodynamic data set for phases of petrological interest. *J Metamorph Geol* 8:89–124
- Holland TJB, Powell R (1998) An internally consistent thermodynamic data set for phases of petrological interest. *J Metamorph Geol* 16:309–343
- Holland TJB, Powell R (2011) An improved and extended internally consistent thermodynamic dataset for phases of petrological interest, involving a new equation of state for solids. *J Metamorph Geol* 29:333–383, doi:10.1111/j.1525–1314.2010.00923.x
- Hollister LS (1966) Garnet zoning: an interpretation based on the Rayleigh fractionation model. *Science* 154:1647–1651

- Hoschek G (2013) Garnet zonation in metapelitic schists from the Eclogite Zone, Tauern Window, Austria: comparison of observed and calculated profiles. *Eur J Mineral* 25:615–629, doi:10.1127/0935-1221/2013/0025-2310
- Indares A, Rivers T (1995) Textures, metamorphic reactions and thermobarometry of eclogitized metagabbros; a Proterozoic example. *Eur J Mineral* 7:43–56
- Janots E, Engi M, Berger A, Allaz J, Schwarz J-O, Spandler C (2008) Prograde metamorphic sequence of REE-minerals in pelitic rocks of the Central Alps: implications for allanite–monazite–xenotime phase relations from 250 to 610 °C. *J Metamorph Geol* 26:509–526, doi:10.1111/j.1525-1314.2008.00774.x
- Johnson CD, Carlson WD (1990) The origin of olivine–plagioclase coronas in metagabbros from the Adirondack Mountains, New York. *J Metamorph Geol* 8:697–717, doi:10.1111/j.1525-1314.1990.tb00496.x
- Johnson TE, Clark C, Taylor RJM, Santosh M, Collins AS (2015) Prograde and retrograde growth of monazite in migmatites: An example from the Nagercoil Block, southern India. *Geosci Front* 6:373–387, doi:10.1016/j.gsf.2014.12.003
- Kelsey DE, Hand M (2015) On ultrahigh temperature crustal metamorphism: Phase equilibria, trace element thermometry, bulk composition, heat sources, timescales and tectonic settings. *Geosci Front* 6:311–356, doi:10.1016/j.gsf.2014.09.006
- Kelsey DE, Powell R (2011) Progress in linking accessory mineral growth and breakdown to major mineral evolution in metamorphic rocks: a thermodynamic approach in the $\text{Na}_2\text{O}-\text{CaO}-\text{K}_2\text{O}-\text{FeO}-\text{MgO}-\text{Al}_2\text{O}_3-\text{SiO}_2-\text{H}_2\text{O}-\text{TiO}_2-\text{ZrO}_2$ system. *J Metamorph Geol* 29:151–166, doi:10.1111/j.1525-1314.2010.00910.x
- Kelsey DE, Clark C, Hand M (2008) Thermobarometric modeling of zircon and monazite growth in melt-bearing systems: examples using model metapelitic and metapsammitic granulites. *J Metamorph Geol* 26:199–212
- Kohn MJ (2009) Models of garnet differential geochronology. *Geochim Cosmochim Acta* 73:170–182, doi:10.1016/j.gca.2008.10.004
- Kohn MJ (2014) 4.7 - Geochemical zoning in metamorphic minerals A2. *In: Treatise on Geochemistry* (Second Edition). Turekian KK, (ed) Elsevier, Oxford, p 249–280
- Kohn MJ (2016) Metamorphic chronology — a tool for all ages: Past achievements and future prospects. *Am Mineral* 101:25–42, doi:10.2138/am-2016-5146
- Kohn MJ, Spear FS (2000) Retrograde net transfer reaction insurance for pressure–temperature estimates. *Geology* 28:1127–1130
- Kohn MJ, Wieland MS, Parkinson CD, Upreti BN (2004) Miocene faulting at plate tectonic velocity in the Himalaya of central Nepal. *Earth Planet Sci Lett* 228:299–310
- Kohn MJ, Wieland MS, Parkinson CD, Upreti BN (2005) Five generations of monazite in Langtang gneisses: implications for chronology of the Himalayan metamorphic core. *J Metamorph Geol* 23:399–406, doi:10.1111/j.1525-1314.2005.00584.x
- Kohn MJ, Corrie SL, Markley C (2015) The fall and rise of metamorphic zircon. *Am Mineral* 100:897–908
- Kohn MJ, Penniston-Dorland SC, Ferreira JC (2016) Implications of near-rim compositional zoning in rutile for geothermometry, geospeedometry, and trace element equilibration. *Contrib Mineral Petrol* 171:78
- Kohn MJ, Penniston-Dorland SC (2017) Diffusion: Obstacles and opportunities in petrochronology. *Rev Mineral Geochem* 83:103–152
- Konrad-Schmolke M, O'Brien PJ, De Capitani C, Carswell DA (2008) Garnet growth at high- and ultra-high pressure conditions and the effect of element fractionation on mineral modes and composition. *Lithos* 103:309–332
- Korhonen FJ, Stout JH (2005) Borosilicate- and phengite-bearing veins from the Grenville Province of Labrador: evidence for rapid uplift. *J Metamorph Geol* 23:297–311, doi:10.1111/j.1525-1314.2005.00577.x
- Korzhinskii DS (1936) Mobility and inertness of components in metasomatism. *Izv Akad Nauk SSSRm Ser Geol* 1:58–60
- Korzhinskii DS (1959) Physicochemical Basis of the Analysis of the Paragenesis of Minerals. Consultants Bureau, New York
- Kriegsman LM, Nyström AI (2003) Melt segregation rates in migmatites: review and critique of common approaches. *Geological Society, London, Special Publications* 220:203–212
- Lanari P, Duesterhoeft E (2016) Thermodynamic modeling using BINGO-ANTIDOTE: A new strategy to investigate metamorphic rocks. *Geophys Res Abstr* 18:EGU2016-11363
- Lanari P, Guillot S, Schwartz S, Vidal O, Tricart P, Riel N, Beyssac O (2012) Diachronous evolution of the alpine continental subduction wedge: evidence from P – T estimates in the Briançonnais Zone houillere (France—Western Alps). *J Geodyn* 56–57:39–54
- Lanari P, Riel N, Guillot S, Vidal O, Schwartz S, Pêcher A, Hattori KH (2013) Deciphering high-pressure metamorphism in collisional context using microprobe mapping methods: Application to the Stak eclogitic massif (northwest Himalaya). *Geology* 41:111–114, doi:10.1130/g33523.1
- Lanari P, Wagner T, Vidal O (2014a) A thermodynamic model for di-trioctahedral chlorite from experimental and natural data in the system $\text{MgO}-\text{FeO}-\text{Al}_2\text{O}_3-\text{SiO}_2-\text{H}_2\text{O}$: applications to P – T sections and geothermometry. *Contr Mineral Petrol* 167–968, doi:10.1007/s00410-014-0968-8

- Lanari P, Rolland Y, Schwartz S, Vidal O, Guillot S, Tricart P, Dumont T (2014b) P - T - t estimation of deformation in low-grade quartz-feldspar-bearing rocks using thermodynamic modelling and $^{40}\text{Ar}/^{39}\text{Ar}$ dating techniques: example of the Plan-de-Phasy shear zone unit (Briançonnais Zone, Western Alps). *Terra Nova* 26:130–138, doi:10.1111/ter.12079
- Lanari P, Vidal O, De Andrade V, Dubacq B, Lewin E, Grosch EG, Schwartz S (2014c) XMapTools: A MATLAB[®]-based program for electron microprobe X-ray image processing and geothermobarometry. *Comp Geosci* 62:227–240, doi:10.1016/j.cageo.2013.08.010
- Lanari P, Giuntoli F, Burn M, Engi M (2017) An inverse modeling approach to obtain P - T conditions of metamorphic stages involving garnet growth and resorption. *Eur J Mineral* in press, doi:10.1127/ejm/2017/0029-2597
- Lasaga AC (1986) Metamorphic reaction rate laws and development of isograds. *Mineral Mag* 50:359–373
- Lasaga AC (1998) *Kinetic Theory in the Earth Sciences*. Princeton University Press, Princeton, New Jersey, 822 p.
- López-Carmona A, Abati J, Pitra P, Lee JKW (2014) Retrogressed lawsonite blueschists from the NW Iberian Massif: P - T - t constraints from thermodynamic modelling and $^{40}\text{Ar}/^{39}\text{Ar}$ geochronology. *Contrib Mineral Petrol* 167:1–20, doi:10.1007/s00410-014-0987-5
- Loury C, Rolland Y, Guillot S, Mikolaichuk AV, Lanari P, Bruguier O, Bosch D (2015) Crustal-scale structure of South Tien Shan: implications for subduction polarity and Cenozoic reactivation. *Geol Soc, London, Spec Publ* 427, doi:10.1144/sp427.4
- Loury C, Rolland Y, Cenki-Tok B, Lanari P, Guillot S (2016) Late Paleozoic evolution of the South Tien Shan: Insights from P - T estimates and allanite geochronology on retrogressed eclogites (Chatkal range, Kyrgyzstan). *J Geodyn* 96:62–80, doi:10.1016/j.jog.2015.06.005
- Mahan KH, Goncalves P, Williams ML, Jercinovic MJ (2006) Dating metamorphic reactions and fluid flow: application to exhumation of high- P granulites in a crustal-scale shear zone, western Canadian Shield. *J Metamorph Geol* 24:193–217, doi:10.1111/j.1525–1314.2006.00633.x
- Manzotti P, Ballèvre M (2013) Multistage garnet in high-pressure metasediments: Alpine overgrowths on Variscan detrital grains. *Geology* 41:1151–1154
- Marmo BA, Clarke GL, Powell R (2002) Fractionation of bulk rock composition due to porphyroblast growth: effects on eclogite facies mineral equilibria, Pam Peninsula, New Caledonia. *J Metamorph Geol* 20:151–165, doi:10.1046/j.0263–4929.2001.00346.x
- Martin AJ, Gehrels GE, DeCelles PG (2007) The tectonic significance of (U,Th)/Pb ages of monazite inclusions in garnet from the Himalaya of central Nepal. *Chem Geol* 244:1–24, doi:10.1016/j.chemgeo.2007.05.003
- Martin C, Debaille V, Lanari P, Goderis S, Vandendael I, Vanhaecke F, Vidal O, Claeys P (2013) REE and Hf distribution among mineral phases in the CV–CK clan: A way to explain present-day Hf isotopic variations in chondrites. *Geochim Cosmochim Acta* 120:496–513, doi:10.1016/j.gca.2013.07.006
- Mészáros M, Hofmann BA, Lanari P, et al. (2016) Petrology and geochemistry of feldspathic impact-melt breccia Abar al' Uj 012, the first lunar meteorite from Saudi Arabia. *Meteorit Planet Sci* 51:1830–1848
- Meyer M, John T, Brandt S, Klemd R (2011) Trace element composition of rutile and the application of Zr-in-rutile thermometry to UHT metamorphism (Epupa Complex, NW Namibia). *Lithos* 126:388–401
- Milord I, Sawyer EW, Brown M (2001) Formation of diatexite migmatite and granite magma during anatexis of semi-pelitic metasedimentary rocks: an Example from St. Malo, France. *J Petrol* 42:487–505, doi:10.1093/petrology/42.3.487
- Miron GD, Wagner T, Kulik DA, Heinrich CA (2016) Internally consistent thermodynamic data for aqueous species in the system Na–K–Al–Si–O–H–Cl. *Geochim Cosmochim Acta* 187:41–78, doi:10.1016/j.gca.2016.04.026
- Montel J-M (1993) A model for monazite/melt equilibrium and application to the generation of granitic magmas. *Chemical Geology* 110:127–146
- Montel J-M, Kornprobst J, Vielzeuf D (2000) Preservation of old U–Th–Pb ages in shielded monazite: example from the Beni Bousera Hercynian kinzigites (Morocco). *J Metamorph Geol* 18:335–342
- Mottram CM, Parrish RR, Regis D, Warren CJ, Argles TW, Harris NBW, Roberts NMW (2015) Using U–Th–Pb petrochronology to determine rates of ductile thrusting: Time windows into the Main Central Thrust, Sikkim Himalaya. *Tectonics* 34:2014TC003743, doi:10.1002/2014TC003743
- Moynihan DP, Pattison DRM (2013) An automated method for the calculation of P - T paths from garnet zoning, with application to metapelitic schist from the Kootenay Arc, British Columbia, Canada. *J Metamorph Geol* 31:525–548, doi:10.1111/jmg.12032
- Netting A, Payne J, Wade B, Raimondo T (2011) Trace element micro-analytical imaging via laser ablation inductively coupled plasma mass spectrometry (LA-ICP-MS). *Microsc Microanal* 17:566–567, doi:10.1017/S1431927611003709
- Orville PM (1969) A model for metamorphic origin of thin layered amphibolites. *Am J Sci* 267:64–86
- Paton C, Hellstrom J, Paul B, Woodhead J, Hergt J (2011) Iolite: Freeware for the visualisation and processing of mass spectrometric data. *J Anal At Spectrom* 26:2508–2518, doi:10.1039/C1JA10172B
- Pattison DRM, De Capitani C, Gaidies F (2011) Petrological consequences of variations in metamorphic reaction affinity. *J Metamorph Geol* 29:953–977, doi:10.1111/j.1525–1314.2011.00950.x

- Paul B, Paton C, Norris A, Woodhead J, Hellstrom J, Hergt J, Greig A (2012) CellSpace: A module for creating spatially registered laser ablation images within the Iolite freeware environment. *J Anal At Spectrom* 27:700–706, doi:10.1039/C2JA10383D
- Paul B, Woodhead JD, Paton C, Hergt JM, Hellstrom J, Norris CA (2014) Towards a method for quantitative LA-ICP-MS imaging of multi-phase assemblages: mineral identification and analysis correction procedures. *Geostand Geoanal Res* 38:253–263, doi:10.1111/j.1751-908X.2014.00270.x
- Peng S, Hu Q, Ewing RP, Liu C, Zachara JM (2012) Quantitative 3-D Elemental Mapping by LA-ICP-MS of a Basaltic Clast from the Hanford 300 Area, Washington, USA. *Environ Sci Technol* 46:2025–2032, doi:10.1021/es2023785
- Pickering-Witter J, Johnston AD (2000) The effects of variable bulk composition on the melting systematics of fertile peridotitic assemblages. *Contrib Mineral Petrol* 140:190–211, doi:10.1007/s004100000183
- Pollington AD, Baxter EF (2010) High resolution Sm–Nd garnet geochronology reveals the uneven pace of tectonometamorphic processes. *Earth Planet Sci Lett* 293:63–71, doi:10.1016/j.epsl.2010.02.019
- Pourteau A, Sudo M, Candan O, Lanari P, Vidal O, Oberhänsli R (2013) Neotethys closure history of Anatolia: insights from ^{40}Ar – ^{39}Ar geochronology and P – T estimation in high-pressure metasedimentary rocks. *J Metamorph Geol* 31:585–606, doi:10.1111/jmg.12034
- Powell R, Downes J (1990) Garnet porphyroblast-bearing leucosomes in metapelites: mechanisms, phase diagrams, and an example from Broken Hill, Australia. *In: High-temperature metamorphism and crustal anatexis*. Springer, p 105–123
- Powell R, Holland TJB (2008) On thermobarometry. *J Metamorph Geol* 26:155–179, doi:10.1111/j.1525–1314.2007.00756.x
- Powell R, Holland T (2010) Using equilibrium thermodynamics to understand metamorphism and metamorphic rocks. *Elements* 6:309–314, doi:10.2113/gselements.6.5.309
- Powell R, Holland T, Worley B (1998) Calculating phase diagrams involving solid solutions via non-linear equations, with examples using THERMOCALC. *J Metamorph Geol* 16:577–588, doi:10.1111/j.1525–1314.1998.00157.x
- Powell R, Guiraud M, White RW (2005) Truth and beauty in metamorphic phase-equilibria: conjugate variables and phase diagrams. *Can Mineral* 43:21–33
- Putnis A (2009) Mineral replacement reactions. *Rev Mineral Geochem* 70:87–124
- Putnis A, John T (2010) Replacement processes in the earth's crust. *Elements* 6:159–164, doi:10.2113/gselements.6.3.159
- Pyle JM, Spear FS (1999) Yttrium zoning in garnet: coupling of major and accessory phases during metamorphic reactions. *Geol Mater Res* 1:1–49
- Pyle JM, Spear FS (2003) Four generations of accessory-phase growth in low-pressure migmatites from SW New Hampshire. *Am Mineral* 88:338–351
- Raimondo T, Payne J, Wade B, Lanari P, Clark C, Hand M (2017) Trace element mapping by LA-ICP-MS: assessing geochemical mobility in garnet. *Contrib Mineral Petrol*, in press.
- Regis D, Rubatto D, Darling J, Cenki-Tok B, Zucali M, Engi M (2014) Multiple metamorphic stages within an eclogite-facies terrane (Sesia Zone, Western Alps) revealed by Th–U–Pb petrochronology. *J Petrol* 55:1429–1456, doi:10.1093/petrology/egu029
- Ridley JR (1984) The significance of deformation associated with blueschist facies metamorphism on the Aegean island of Syros. *In: The Geological Evolution of the Eastern Mediterranean*. Vol 17. Dixon JE, Robertson AHF (eds) Geological Society, 545–550
- Riel N, Lanari P (2015) Techniques, méthodes et outils pour la quantification du métamorphisme. *Géochroniques* 136:53–60
- Rittner M, Müller W (2012) 2D mapping of LA-ICPMS trace element distributions using R. *Comput Geosci* 42:152–161, doi:10.1016/j.cageo.2011.07.016
- Roberts MP, Finger F (1997) Do U–Pb zircon ages from granulites reflect peak metamorphic conditions? *Geology* 25:319–322, doi:10.1130/0091-7613(1997)025<0319:dupzaf>2.3.co;2
- Robyr M, Darbellay B, Baumgartner LP (2014) Matrix-dependent garnet growth in polymetamorphic rocks of the Sesia zone, Italian Alps. *J Metamorph Geol* 32:3–24, doi:10.1111/jmg.12055
- Rubatto D (2017) Zircon: The metamorphic mineral. *Rev Mineral Geochem* 83:261–295
- Rubatto D, Hermann J, Buick IS (2006) Temperature and bulk composition control on the growth of monazite and zircon during low-pressure anatexis (Mount Stafford, Central Australia). *J Petrol* 47:1973–1996, doi:10.1093/petrology/egl033
- Sayab M (2006) Decompression through clockwise P – T path: implications for early N–S shortening orogenesis in the Mesoproterozoic Mt Isa Inlier (NE Australia). *J Metamorph Geol* 24:89–105, doi:10.1111/j.1525–1314.2005.00626.x
- Scheffer C, Vanderhaeghe O, Lanari P, Tarantola A, Ponthus L, Photiades A, France L (2016) Syn- to post-orogenic exhumation of metamorphic nappes: Structure and thermobarometry of the western Attic-Cycladic metamorphic complex (Lavrion, Greece). *J Geodyn* 96:174–193, doi:10.1016/j.jog.2015.08.005

- Schorn S, Diener JFA (2016) Details of the gabbro-to-eclogite transition determined from microtextures and calculated chemical potential relationships. *J Metamorph Geol*, doi:10.1111/jmg.12220
- Schwarz J-O, Engi M, Berger A (2011) Porphyroblast crystallization kinetics: The role of the nutrient production rate. *J Metamorph Geol* 29, doi:10.1111/j.1525-1314.2011.00927.x
- Šelih VS, van Elteren JT (2011) Quantitative multi-element mapping of ancient glass using a simple and robust LA-ICP-MS rastering procedure in combination with image analysis. *Anal Bioanal Chem* 401:745–755, doi:10.1007/s00216-011-5119-8
- Selverstone J, Spear FS (1985) Metamorphic P – T Paths from pelitic schists and greenstones from the south-west Tauern Window, Eastern Alps. *J Metamorph Geol* 3:439–465, doi:10.1111/j.1525-1314.1985.tb00329.x
- Sousa J, Kohn MJ, Schmitz MD, Northrup CJ, Spear FS (2013) Strontium isotope zoning in garnet: implications for metamorphic matrix equilibration, geochronology and phase equilibrium modelling. *J Metamorph Geol* 31:437–452, doi:10.1111/jmg.12028
- Spear FS (1988a) The Gibbs method and Duhem's theorem: The quantitative relationships among P , T , chemical potential, phase composition and reaction progress in igneous and metamorphic systems. *Contrib Mineral Petrol* 99:249–256, doi:10.1007/bf00371465
- Spear FS (1988b) Metamorphic fractional crystallization and internal metasomatism by diffusional homogenization of zoned garnets. *Contrib Mineral Petrol* 99:507–517, doi:10.1007/bf00371941
- Spear FS (1991) On the interpretation of peak metamorphic temperatures in light of garnet diffusion during cooling. *J Metamorph Geol* 9:379–388, doi:10.1111/j.1525-1314.1991.tb00533.x
- Spear FS (1993) Metamorphic Phase Equilibria and Pressure–temperature–Time Paths. Monograph Mineral Soc Am, Washington, D.C.
- Spear FS, Daniel CG (2001) Diffusion control of garnet growth, Harpswell Neck, Maine, USA. *J Metamorph Geol* 19:179–195
- Spear FS, Kohn MJ (1996) Trace element zoning in garnet as a monitor of crustal melting. *Geology* 24:1099–1102
- Spear FS, Pyle JM (2010) Theoretical modeling of monazite growth in a low-Ca metapelite. *Chem Geol* 273:111–119
- Spear FS, Selverstone J (1983) Quantitative P – T paths from zoned minerals: Theory and applications. *Contrib Mineral Petrol* 83:348–357
- Spear FS, Selverstone J, Hickmott D, Crowley P, Hodges KV (1984) P – T paths from garnet zoning: A new technique for deciphering tectonic processes in crystalline terranes. *Geology* 12:87–90
- Spear FS, Kohn MJ, Florence FP, Menard T (1990) A model for garnet and plagioclase growth in pelitic schists: implications for thermobarometry and P – T path determinations. *J Metamorph Geol* 8:683–696, doi:10.1111/j.1525-1314.1990.tb00495.x
- Spear FS, Kohn MJ, Florence FP, Menard T (1991) A model for garnet and plagioclase growth in pelitic schists: Implications for thermobarometry and P – T path determinations. *J Metamorph Geol* 8:683–696
- Spear FS, Thomas JB, Hallett BW (2014) Overstepping the garnet isograd: a comparison of QuiG barometry and thermodynamic modeling. *Contrib Mineral Petrol* 168:1–15
- Spear FS, Pattison DRM, Cheney JT (2016) The metamorphism of metamorphic petrology. *Geol Soc Am Spec Papers* 523, doi:10.1130/2016.2523(02)
- Stepanov AS, Hermann J, Rubatto D, Rapp RP (2012) Experimental study of monazite/melt partitioning with implications for the REE, Th and U geochemistry of crustal rocks. *Chem Geol* 300–301:200–220, doi:10.1016/j.chemgeo.2012.01.007
- Stevens G, Clemens JD, Droop GTR (1997) Melt production during granulite-facies anatexis: experimental data from “primitive” metasedimentary protoliths. *Contrib Mineral Petrol* 128:352–370, doi:10.1007/s004100050314
- Stowell H, Tulloch A, Zuluaga C, Koenig A (2010) Timing and duration of garnet granulite metamorphism in magmatic arc crust, Fiordland, New Zealand. *Chem Geol* 273:91–110, doi:10.1016/j.chemgeo.2010.02.015
- Stüwe K (1997) Effective bulk composition changes due to cooling: a model predicting complexities in retrograde reaction textures. *Contrib Mineral Petrol* 129:43–52, doi:10.1007/s004100050322
- Taylor-Jones K, Powell R (2015) Interpreting zirconium-in-rutile thermometric results. *J Metamorph Geol* 33:115–122
- Thompson J (1959) Local equilibrium in metasomatic processes. *In: Researches in Geochemistry* 1, Abelson PH (Ed) Wiley, New York, p. 427–457
- Thompson JB (1955) The thermodynamic basis for the mineral facies concept. *Am J Sci* 253:65–103, doi:10.2475/ajs.253.2.65
- Thompson JB (1970) Geochemical reaction and open systems. *Geochim Cosmochim Acta* 34:529–551, doi:10.1016/0016-7037(70)90015-3
- Tinkham DK, Ghent ED (2005a) Estimating P – T conditions of garnet growth with isochemical phase-diagrams sections and the problem of effective bulk-composition. *Can Mineral* 43:35–50, doi:10.2113/gscanmin.43.1.35
- Tinkham DK, Ghent ED (2005b) XRMMapAnal: A program for analysis of quantitative X-ray maps. *Am Mineral* 90:737–744, doi:10.2138/am.2005.1483
- Tinkham DK, Zuluaga CA, Stowell HH (2001) Metapelite phase equilibria modeling in MnNCKFMASH: The effect of variable Al_2O_3 and $MgO/(MgO+FeO)$ on mineral stability. *Geol Mater Res* 3:1–42
- Tóth M, Grandjean V, Engi M (2000) Polyphase evolution and reaction sequence of compositional domains in metabasalt: A model based on local chemical equilibrium and metamorphic differentiation. *Geol J* 35:163–183

- Tracy RJ (1982) Compositional zoning and inclusions in metamorphic minerals. *Rev Mineral Geochem* 10:355–397
- Tracy RJ, Robinson P, Thompson AB (1976) Garnet composition and zoning in the determination of temperature and pressure of metamorphism, central Massachusetts. *Am Mineral* 61:762–775
- Trincal V, Lanari P, Buatier M, Lacroix B, Charpentier D, Labaume P, Muñoz M (2015) Temperature micro-mapping in oscillatory-zoned chlorite: Application to study of a green-schist facies fault zone in the Pyrenean Axial Zone (Spain). *Am Mineral* 100:2468–2483, doi:10.2138/am-2015-5217
- Tropper P, Manning CE, Harlov DE (2011) Solubility of CePO_4 monazite and YPO_4 xenotime in H_2O and $\text{H}_2\text{O}-\text{NaCl}$ at 800 °C and 1 GPa: Implications for REE and Y transport during high-grade metamorphism. *Chem Geol* 282:58–66, doi:10.1016/j.chemgeo.2011.01.009
- Ubide T, McKenna CA, Chew DM, Kamber BS (2015) High-resolution LA-ICP-MS trace element mapping of igneous minerals: In search of magma histories. *Chem Geol* 409:157–168, doi:10.1016/j.chemgeo.2015.05.020
- Vance D, Mahar E (1998) Pressure–temperature paths from PT pseudosections and zoned garnets: potential, limitations and examples from the Zaskar Himalaya, NW India. *Contrib Mineral Petrol* 132:225–245
- Verdecchia SO, Reche J, Baldo EG, Segovia-Diaz E, Martinez FJ (2013) Staurolite porphyroblast controls on local bulk compositional and microstructural changes during decompression of a St–Bt–Grt–Crd–And schist (Ancasti metamorphic complex, Sierras Pampeanas, W Argentina). *J Metamorph Geol* 31:131–146, doi:10.1111/jmg.12003
- Vernon RH (1989) Porphyroblast-matrix microstructural relationships: recent approaches and problems. *Geol Soc, London, Spec Publ* 43:83–102, doi:10.1144/gsl.sp.1989.043.01.05
- Vernon RH, Collins WJ (1988) Igneous microstructures in migmatites. *Geology* 16:1126–1129, doi:10.1130/0091-7613(1988)016<1126:imim>2.3.co;2
- Vidal O, De Andrade V, Lewin E, Munoz M, Parra T, Pascarelli S (2006) P – T -deformation– $\text{Fe}^{3+}/\text{Fe}^{2+}$ mapping at the thin section scale and comparison with XANES mapping: application to a garnet-bearing metapelite from the Sambagawa metamorphic belt (Japan). *J Metamorph Geol* 24:669–683, doi:10.1111/j.1525-1314.2006.00661.x
- Vitale Brovarone A, Beltrando M, Malavieille J, Giuntoli F, Tondella E, Groppo C, Beyssac O, Compagnoni R (2011) Inherited Ocean–Continent Transition zones in deeply subducted terranes: Insights from Alpine Corsica. *Lithos* 124:273–290, doi:10.1016/j.lithos.2011.02.013
- Vrijmoed JC, Hacker BR (2014) Determining P – T paths from garnet zoning using a brute-force computational method. *Contrib Mineral Petrol* 167:1–13, doi:10.1007/s00410-014-0997-3
- Warren CJ, Waters DJ (2006) Oxidized eclogites and garnet-blueschists from Oman: P – T path modelling in the NCFMASHO system. *J Metamorph Geol* 24:783–802, doi:10.1111/j.1525-1314.2006.00668.x
- Waters DJ, Lovegrove DP (2002) Assessing the extent of disequilibrium and overstepping of prograde metamorphic reactions in metapelites from the Bushveld Complex aureole, South Africa. *J Metamorph Geol* 20:135–149, doi:10.1046/j.0263-4929.2001.00350.x
- White RW, Powell R (2010) Retrograde melt–residue interaction and the formation of near-anhydrous leucosomes in migmatites. *J Metamorph Geol* 28:579–597, doi:10.1111/j.1525-1314.2010.00881.x
- White RW, Powell R, Holland TJB (2001) Calculation of partial melting equilibria in the system $\text{Na}_2\text{O}-\text{CaO}-\text{K}_2\text{O}-\text{FeO}-\text{MgO}-\text{Al}_2\text{O}_3-\text{SiO}_2-\text{H}_2\text{O}$ (NCKFMASH). *J Metamorph Geol* 19:139–153, doi:10.1046/j.0263-4929.2000.00303.x
- White RW, Powell R, Clarke GL (2003) Prograde Metamorphic Assemblage evolution during partial melting of metasedimentary rocks at low pressures: Migmatites from Mt Stafford, Central Australia. *J Petrol* 44:1937–1960, doi:10.1093/petrology/egg065
- White RW, Powell R, Baldwin JA (2008) Calculated phase equilibria involving chemical potentials to investigate the textural evolution of metamorphic rocks. *J Metamorph Geol* 26:181–198, doi:10.1111/j.1525-1314.2008.00764.x
- White WM (2013) *Geochemistry*. Wiley-Blackwell
- Whitehouse MJ, Platt JP (2003) Dating high-grade metamorphism—constraints from rare-earth elements in zircon and garnet. *Contrib Mineral Petrol* 145:61–74, doi:10.1007/s00410-002-0432-z
- Whitney DL, Evans BW (2010) Abbreviations for names of rock-forming minerals. *Am Mineral* 95:185–187, doi:10.2138/am.2010.3371
- Williams ML (1994) Sigmoidal inclusion trails, punctuated fabric development, and interactions between metamorphism and deformation. *J Metamorph Geol* 12:1–21, doi:10.1111/j.1525-1314.1994.tb00001.x
- Williams ML, Jercinovic MJ, Hetherington CJ (2007) Microprobe monazite geochronology: Understanding geologic processes by integrating composition and chronology. *Ann Rev Earth Planet Sci* 35:137–175, doi:10.1146/annurev.earth.35.031306.140228
- Williams ML, Jercinovic MJ, Mahan KH, Dumond G (2017) Electron microprobe petrochronology. *Rev Mineral Geochem* 83:153–182
- Wing BA, Ferry JM, Harrison TM (2003) Prograde destruction and formation of monazite and allanite during contact and regional metamorphism of pelites: petrology and geochronology. *Contrib Mineral Petrol* 145:228–250

- Wintsch RP (1985) The possible effects of deformation on chemical processes in metamorphic fault zones. *In: Metamorphic Reactions: Kinetics, Textures, and Deformation*. Thompson AB, Rubie DC (eds). Springer New York, New York, NY, p 251–268
- Woodhead JD, Hellstrom J, Hergt JM, Greig A, Maas R (2007) Isotopic and elemental imaging of geological materials by laser ablation inductively coupled plasma-mass spectrometry. *Geostand Geoanal Res* 31:331–343, doi:10.1111/j.1751-908X.2007.00104.x
- Yakymchuk C, Brown M (2014) Behaviour of zircon and monazite during crustal melting. *J Geol Soc* 171:465–479, doi:10.1144/jgs2013-115
- Yakymchuk C, Clark C, White RW (2017) Phase relations, reaction sequences and petrochronology. *Rev Mineral Geochem* 83:13–53
- Yamato P, Agard P, Burov E, Le Pourhiet L, Jolivet L, Tiberi C (2007) Burial and exhumation in a subduction wedge: Mutual constraints from thermomechanical modeling and natural P – T – t data (Schistes Lustrés, western Alps). *J Geophys Res: Solid Earth* 112:B07410, doi:10.1029/2006JB004441
- Zack T, Kooijman E (2017) Petrology and geochronology of rutile. *Rev Mineral Geochem* 83:443–467
- Zeh A (2006) Calculation of garnet fractionation in metamorphic rocks, with application to a flat-top, Y-rich garnet population from the Ruhla Crystalline Complex, Central Germany. *J Petrol* 47:2335–2356, doi:10.1093/petrology/egl046
- Zhang L, Wang Q, Song S (2009) Lawsonite blueschist in Northern Qilian, NW China: P – T pseudosections and petrologic implications. *J Asian Earth Sci* 35:354–366, doi:10.1016/j.jseas.2008.11.007
- Zuluaga CA, Stowell HH, Tinkham DK (2005) The effect of zoned garnet on metapelite pseudosection topology and calculated metamorphic P – T paths. *Am Mineral* 90:1619–1628, doi:10.2138/am.2005.1741